The Canadian Mineralogist
Vol. 52, pp. 373-397 (2014)
DOI: 10.3749/canmin.52.2.373

MINERALOGY AND PETROGRAPHY OF PHOSPHATE MINERAL ASSOCIATIONS FROM THE JOCÃO PEGMATITE, MINAS GERAIS, BRAZIL

MAXIME BAIJOT, FRÉDÉRIC HATERT[§], AND FABRICE DAL BO

Laboratoire de Minéralogie, B18, Université de Liège, B-4000 Liège, Belgium

SIMON PHILIPPO

Section Minéralogie, Musée national d'histoire naturelle, Rue Münster 25, L-2160 Luxembourg, Grand-Duché de Luxembourg

ABSTRACT

The Jocão pegmatite (or Cigana) is located in the well-known Eastern Brazilian Pegmatitic Province (EBPP), Minas Gerais, Brazil. According to their macroscopic textures, three different kinds of phosphate mineral masses were collected from the dumps of the pegmatite: association I is composed of dendritic triphylite, forming intergrowths with silicate minerals (spessartine garnet or albite); association II forms blocky nodules of triphylite-ferrisicklerite-heterosite; and association III shows exsolution lamellae of ferrisicklerite-heterosite in massive beusite. The primary textures and the Fe/(Fe+Mn) ratios of primary triphylite make it possible to establish the crystallization sequence of the primary phases; the petrogenesis of primary intergrowths between garnet and triphylite of association I is also discussed. In the three associations, these primary minerals are hydrothermally altered and secondary species are produced. In association I, the first hydrothermal alteration event was a weakly oxidizing hydroxylation stage, during which triphylite was only replaced by hureaulite (rarely associated with barbosalite) along its cleavage planes. The final stage affecting association I corresponds to meteoric processes during which ludlamite and then vivianite progressively replaced triphylite. Association II evolved under more oxidizing conditions and the first alteration stage corresponds to the progressive oxidation of triphylite accompanied by Li-leaching, leading to ferrisicklerite and heterosite. The second hydrothermal stage corresponds to a hydroxylation event, and the secondary species depend on the phosphate mineral that they replace: triphylite is only altered to Fe^{2+}-Mn^{2+}-bearing hydrated species (colorless hureaulite); ferrisicklerite is altered to Fe^{2+}-, Mn^{2+}-, and Fe^{3+}-bearing phosphate minerals such as jahnsite *s.l.*, frondelite *s.l.*, and orange hureaulite; heterosite is replaced by Fe^{3+}-bearing species such as ferristrunzite. Consequently, it appears that the secondary phosphate minerals, which crystallize during this second hydrothermal stage, strongly depend on the cations which are locally available in the sample zone. The final stage forms the meteoric species: leucophosphite and phosphosiderite directly replace heterosite, whereas vivianite, a ferrous meteoric species, only appears in the triphylite core. In association III, exsolution lamellae are formed at the expense of a high-temperature homogenous Ca-Li-bearing graftonite-beusite-like phase; when the temperature decreased, Li migrated into triphylite and Ca to the larger M1 site of beusite. During the high-temperature hydrothermal alteration processes, triphylite transforms into ferrisicklerite and heterosite, like in association II; however, beusite is not affected by any transformation process at that stage. During the low temperature hydroxylation stage, ferrisicklerite from the core remains almost unaltered, while beusite is replaced by an intimate mixture of pleochroic Ca-rich hureaulite and tavorite. After this hydroxylation stage, the meteoric stage is characterized by an increase in Ca^{2+} and H_2O activities, responsible for the replacement of hureaulite and tavorite by mitridatite-robertsite. At the nodule border, beusite and heterosite are completely replaced by an intimate mixture mainly composed of frondelite and robertsite-mitridatite. Finally, this study shows that the small phosphate nodules from Jocão are more affected by oxidation than large nodules, thus indicating that the diffusion kinetics of hydrothermal fluids is relatively low in these phosphate nodules. As a consequence, large phosphate nodules show a typical zoning with triphylite (core)–ferrisicklerite-heterosite (rim); this zoning, which preserves the crystal structure of the phosphate minerals, was achieved during the high temperature hydrothermal transformations. The phosphate nodules consequently appear as a relatively closed system compared to the silicate matrix.

Keywords: Fe-Mn phosphates, primary textures, genetic sequence, secondary phosphates, Jocão pegmatite, Brazil

§ *E-mail address:* fhatert@ulg.ac.be

Introduction

One of the most important pegmatite provinces in the world, the Eastern Brazilian Pegmatite Province (EBPP), is located on the east side of the Saõ Francisco craton, mainly in the state of Minas Gerais, in Brazil. It also encompasses the states of Bahia, Espírito Santo, and Rio de Janeiro (Paiva 1946, Putzer 1976, Correia Nevez *et al*. 1986). In September 2008 and July 2010, we visited several pegmatites located in the Conselheiro Pena district, between Galiléia and Mendes Pimentel (Fig. 1), in order to investigate the mineralogy and petrography of phosphate minerals, as well as their textural relationships with the associated silicates.

Among these pegmatites, the Jocão pegmatite presents complex phosphate mineral associations, showing blocky or dendritic habits. This latter texture sometimes involves intergrowths of triphylite and silicate minerals (spessartine or albite). Moreover, spessartine and triphylite also present different petrographic relationships: rims of triphylite around spessartine, enclosed grains of spessartine in triphylite, or rims of spessartine around triphylite. In pegmatites, Fe-Mn-bearing silicate minerals rarely crystallize in close association with Fe-Mn-bearing phosphate minerals; nevertheless, Vignola *et al*. (2011) found two different petrographic textures involving silicate minerals (garnet) and phosphate minerals (graftonite, triphylite) in the Luna pegmatitic dike, Italian Alps.

The aims of this present paper are (1) to investigate in detail the petrographic relationships among phosphate minerals as well as their chemical variations, (2) to better understand the transformation sequences which affected these minerals, (3) to discuss and explain the different kinds of phosphate mineral habits (blocky, dendritic, exsolutions) and their genetic significance at the pegmatite scale, and (4) to determine the processes responsible for the formation of complex triphylite-spessartine intergrowths.

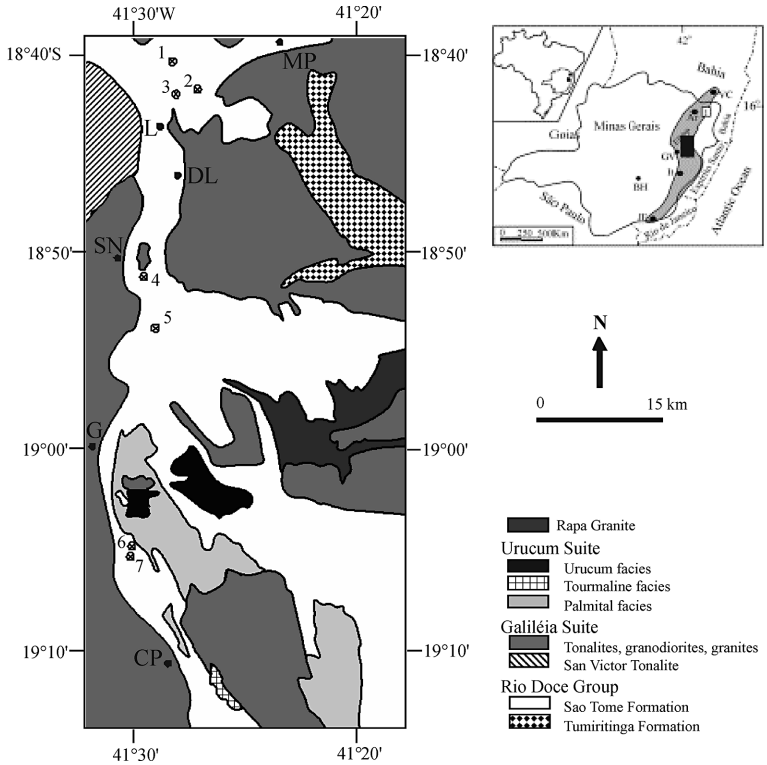

FIG. 1 Geological map of Conselheiro Pena District (modified from Nalini *et al*. 2000, Chaves *et al*. 2005, Chaves & Scholz 2008). Localities: MP = Mendes Pimentel, L = Linópolis, DL = Divino das Larenjeiras, SN = Sapucaia do Norte, G = Galiléia, CP = Conselheiro Pena. Investigated pegmatites: 1 = Telírio, 2 = Sebastião Cristino, 3 = Jaime, 4 = Boca Rica, 5 = Sapucaia, 6 = Jocão (Cigana), 7 = Noa Boa Vista.

Geological Setting

The Eastern Brazilian Pegmatite Province (EBPP) is divided into several districts, among which is the Conselheiro Pena district (Pedrosa-Soares *et al*. 2009, 2011), which consists of a gneissic and migmatitic basement dated from Archean to Lower Proterozoic (Procrane and Piedade complex, Nalini *et al*. 2000). The Late Proterozoic cover consists of amphibolite-facies rocks, such as sillimanite-staurolite-garnet-mica-bearing schists (Rio Doce Group), with intercalations of micaceous quartzites (Crenaque Group) (Nalini 1997, Nalini *et al*. 2000). Most pegmatites in the EBPP originated with one of the pre-, syn-, and post-tectonic granitoids that were emplaced during the 630–480 My Brazilian orogeny (Pedrosa-Soares *et al*. 2011). Two of these intrusions crosscut the cover and the basement rocks of the Conselheiro Pena district: the Galiléia and Urucum magmatic suites, which belong to the G1 (630–585 My) and G2 (585–560 My) supersuites, respectively (Pedrosa-Soares *et al*. 2001, 2009). The Galiléia granitoid (595 My) is a metaluminous suite characterized by a polydiapiric batholith, consisting mainly of granodiorites and tonalites with minor granites. These rocks are associated with the pre-collisional magmatism of the Brazilian orogeny, and have calc-alkaline affinities (Nalini *et al*. 2000, Pedrosa-Soares *et al*. 2001, 2009, 2011). The Urucum suite (582 My) is composed of four different types of rocks: a granite containing megacrysts of feldspar (Urucum facies), a medium- to coarse-grained granite (Palmital facies), a tourmaline-bearing granite, and a pegmatitic granite (Nalini 1997). These rocks generally show a peraluminous composition (S-type granite) due to the syncollisional character of the orogeny (Nalini *et al*. 2000, Pedrosa-Soares *et al*. 2001, 2011).

The Jocão pegmatite, also called Cigana or Boavista Cigana, is located on the left side of the Rio Doce River, 10 km SSE of the town of Galiléia (19°4'30" S; 41°29'20" O; Fig. 1). This elliptic pegmatite (40 m in length, 30 m in width, and 20 m high) intruded the subvertical mica schists of the Sao Tomé formation. Even though part of the pegmatite was under water, we were able to collect complex phosphate mineral associations from the dumps, as well as associated silicate minerals, which are listed in Table 1. The silicate matrix mainly consists of saccharoidal albite (± quartz), or quartz and K-feldpsar which sometimes show graphic intergrowths. Schorl occurs in this matrix and some crystals reach 10 cm in length. Reddish garnet forms masses up to 5 cm in diameter, enclosed in saccharoidal albite or in quartz + K-feldspar matrix. These are frequently surrounded by a limpid rim of quartz (0.5 to 1 cm in width). The garnets are always associated with apatite and sometimes with triphylite. The muscovite shows a fishbone-like habit, in which the crystals can reach 15 cm in length, while some of smaller micas (flakes 1 cm in length) exhibit a yellowish color and occasionally occur in cracks. Hexagonal prisms of beryl, reaching 3 cm in length, translucent yellowish spodumene, columbite-group minerals, and löllingite were also found in the dumps. The presence of saccharoidal albite and cleavelandite indicate that this pegmatite was affected by albitization processes.

Three types of phosphate associations were found in the Jocão pegmatite. The first association (I) consists of dendritic and skeletal textures involving triphylite and albite (Fig. 2a) or garnet (Fig. 2b) and forming complex intergrowths. Quartz and apatite may be associated as accessory minerals (Figs. 2b, c). Triphylite often has a bluish color due to partial alteration to vivianite. The second association (II) occurs as nodules (15 × 15 cm) covered by oxide minerals, showing a core constituted of massive fresh greyish to bluish triphylite, which becomes more and more altered by secondary phosphate minerals when approaching the oxide rim. This mineral zonation is underlined by the different colors of the "Quensel-Mason" phosphates: greenish for triphylite (core), brownish for ferrisicklerite (transition zone), purple for heterosite (external zone), and finally a dark color for the oxide minerals (rim). The third association (III) also consists of a nodule covered by oxide minerals; this nodule is larger (70 × 50 cm) and shows intergrowths between ferrisicklerite (brownish lamellae maximum 1 mm in thickness) and a reddish massive beusite. It is noteworthy that these lamellae become purplish on the border of the nodule, due to their transformation to heterosite. Perched on the oxide border there occurs a yellowish to greenish uraniferous crust of saléeite, associated with octahedra of gahnite.

Analytical Methods

Mineral identification is based on the observations of thin sections under the polarizing microscope, as well as on X-ray powder diffraction measurements, which were acquired with Panalytical PW 3710 (Fe$K\alpha$ radiation, λ = 1.9373 Å) and Panalytical PW1730 (Debye-Scherrer method, Cu$K\alpha$ radiation, λ = 1.5418 Å) diffractometers.

Quantitative chemical analyses were performed with a Cameca SX-100 electron microprobe (Institut für Mineralogie und Kristallchemie, Universität Stuttgart, Germany) operating in the wavelength-dispersion mode, with an accelerating voltage of 15 kV, a beam current of 10 nA, and a beam diameter of 5 μm. The following standards were used: graftonite (P), wollastonite (Si, Ca), corundum (Al), periclase (Mg), sphalerite (Zn), hematite (Fe), rhodonite (Mn), albite (Na), orthoclase (K) and synthetic BaF_2 (F).

Mineralogical and Petrographic Descriptions

Our investigation revealed the presence of 40 minerals in the phosphate masses from Jocão, among which are 27 phosphate, 8 associated silicate, 3 oxide,

TABLE 1. FORMULAE AND RELATIVE ABUNDANCES OF MINERALS FROM THE THREE ASSEMBLAGES, JOCÃO PEGMATITE, MINAS GERAIS, BRAZIL

Mineral name	Formula	Abundance Ass. I	Ass. II	Ass. III
Primary phosphate minerals				
Triphylite	$Li(Fe^{2+},Mn^{2+})PO_4$	xxx	xx	o
Beusite	$(Mn,Fe,Ca)_3(PO_4)_2$	o	o	xxx
Fluorapatite	$Ca_5(PO_4)_3F$	xx	o	o
Secondary phosphate minerals				
Ferrisicklerite	$Li_{<1}(Fe^{3+},Mn^{2+})PO_4$	o	xx	xx
Heterosite	$(Fe^{3+},Mn^{3+})PO_4$	o	xx	xxx
Hydroxylapatite	$Ca_5(PO_4)_3OH$	x	o	o
Fluorapatite	$Ca_5(PO_4)_3F$	o	o	xx
Frondelite	$Mn^{2+}Fe^{3+}_4(PO_4)_3(OH)_5$	x	xx	o
Rockbridgeite	$Fe^{2+}Fe^{3+}_4(PO_4)_3(OH)_5$	x	xx	o
Jahnsite-(MnMnMn)	$MnMn^{2+}Mn_2Fe^{3+}_2(PO_4)_4(OH)_2•8H_2O$	o	xx	o
"Jahnsite-(MnMnFe^{2+})" *	$MnMn^{2+}Fe^{2+}_2Fe^{3+}_2(PO_4)_4(OH)_2•8H_2O$	x	o	o
"Whiteite-(MnMnMg)" *	$MnMnMg_2Al_2(PO_4)_4(OH)_2•8H_2O$	x	o	o
Hureaulite	$(Mn^{2+})_5(PO_3OH)_2(PO_4)_2•4H_2O$	xxx	xx	xx
Barbosalite	$Fe^{2+}(Fe^{3+})_2(PO_4)_2(OH)_2$	xx	xxx	o
Tavorite	$LiFe^{3+}(PO_4)(OH)$	x	x	xx
Lipscombite	$Fe^{2+}(Fe^{3+})_2(PO_4)_2(OH)_2$	x	o	x
Harrisonite	$Ca(Fe^{2+},Mg)_6(PO_4)_2(SiO_4)_2$	o	o	x
Leucophosphite	$KFe^{3+}_2(PO_4)_2(OH)•2H_2O$	o	x	x
Phosphosiderite	$Fe^{3+}PO_4•2H_2O$	o	x	x
Robertsite	$Ca_2Mn^{3+}_3(PO_4)_3O_2•3H_2O$	o	o	xx
Mitridatite	$Ca_2Fe^{3+}_3(PO_4)_3O_2•3H_2O$	o	o	xx
Ferristrunzite	$Fe^{3+}Fe^{3+}_2(PO_4)_2(OH)_3•5H_2O$	o	x	o
Vivianite	$Fe^{2+}(PO_4)•8H_2O$	xxx	xx	o
Ludlamite	$(Fe^{2+})_3(PO_4)_2•4H_2O$	x	x	o
Greifensteinite	$Ca_2Fe^{2+}_5Be_4(PO_4)_6(OH)_4•6H_2O$	x	o	o
Staněkite	$Fe^{3+}(Mn^{2+},Fe^{2+},Mg)(PO_4)O$	o	o	x
Saléeite	$Mg(UO)_2(PO_4)_2•10H_2O$	o	o	x
Associated silicate, oxide, and sulfide minerals				
Albite	$NaAlSi_3O_8$	xxx	xx	o
Microcline	$KAlSi_3O_8$	x	o	o
Quartz	SiO_2	xx	xx	o
Schorl	$Na(Fe^{2+})_3Al_6(BO_3)_3Si_6O_{18}(OH)_4$	x	o	o
Muscovite	$KAl_2(Si_3Al)O_{10}(OH)_2$	xx	x	o
Spessartine	$(Mn,Fe^{2+})_3Al_2(SiO_4)_3$	xx	o	x
Chamosite	$(Fe^{2+},Mg,Al,Fe^{3+})_6(Si,Al)_4O_{10}(OH,O)_8$	x	x	o
Zircon	$Zr(SiO_4)$	x	o	o
Mn- and Fe-bearing oxides	-	x	xx	xx
Gahnite	$ZnAl_2O_4$	o	o	x
Sphalerite	(Zn,Fe)S	o	x	o
Pyrite	FeS_2	x	o	o
U- and Bi- bearing oxides	-	x	o	o

* Species not approved by IMA-CNMNC
xxx = abundant ; xx = less abundant ; x= scarce ; o = absent

and 2 sulfide minerals. These minerals, as well as their chemical formulae and abundances, are given in Table 1. Moreover, all the investigated samples from Jocão are listed in Table 2, in which the phosphate mineral associations are briefly described. All minerals described below were analyzed with the electron microprobe; the complete set of chemical data is available from the Depository of Unpublished Data on the Mineralogical Association of Canada website (document CM52_373).

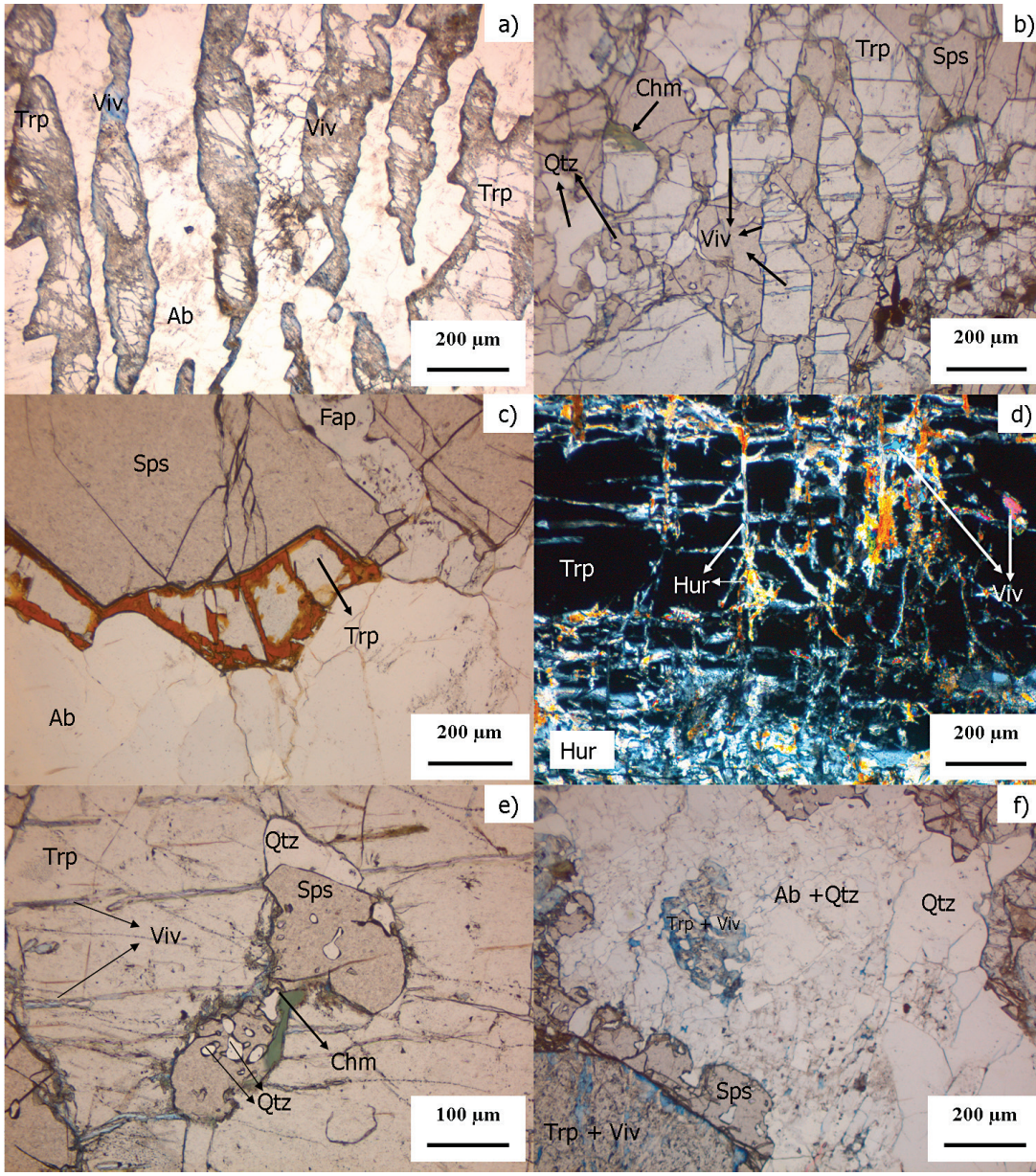

FIG. 2. Phosphate minerals from association I. (a) Skeletal triphylite (Trp) into albite (Ab). Triphylite is intensively replaced by vivianite (Viv). Association I, Joc-3, plane-polarized light. (b) Intergrowths between spessartine garnet (Sps) and triphylite. Vivianite and chamosite (Chm) appear between grain boundaries. Chamosite may also crystallize in cracks within spessartine garnet, and vivianite in cleavage planes of triphylite. Quartz (Qtz) is generally enclosed in garnet grains. Association I, Joc-10a, plane-polarized light. (c) Rim of triphylite around spessartine. Fluorapatite (Fap) occurs in cracks within garnet and in the albite matrix. The orange mineral is an undetermined Fe-Mn bearing phosphate. Association I, Joc-12, plane-polarized light. (d) Cellular texture in triphylite. This mineral is replaced along its perpendicular cleavage planes by colorless hureaulite (Hur) and vivianite. On the bottom, triphylite is completely replaced by hureaulite. Association I, Cig-1, crossed polars. (e) Spessartine grain (Sps) enclosed in triphylite (Trp) and exhibiting symplectic texture with quartz (Qtz). Chamosite (Chm) and vivianite replace spessartine and vivianite, respectively. Association I, Joc-10a, plane-polarized light. (f) Rim of spessartine around triphylite intensively altered by vivianite (Viv). The matrix is composed of albite (Ab) and quartz. Association I, Joc-10a, plane-polarized light.

TABLE 2. PETROGRAPHIC DESCRIPTION OF PHOSPHATE SAMPLES FROM THE JOCÃO PEGMATITE, BRAZIL

Samples	T a	Phosphate minerals	Main petrographic texture
PU-076	I	Trp + viv	Dendritic triphylite + albite + quartz (± muscovite); vivianite in the cleavage planes and around triphylite grains
CIG-1	I	Trp + hur ± viv	Dendritic triphylite + albite + quartz (± muscovite); hureaulite in cleavage planes of triphylite forming cellular texture (Fig. 2d)
CIG-26-07	I	Trp + viv	Dendritic triphylite + albite + quartz (± muscovite); vivianite in the cleavage planes of triphylite, forming cellular texture
Joc-1	I	Fap + Rock-fnd + " jahn-(MnMnFe^{2+}) " + "whit-(MnMnMg)"	Accessory intergranular phosphates occurring between "cleavelandite" grains
Joc-3	I	Trp+ viv + hur ± lud ± fap	Dendritic triphylite + albite + quartz (± muscovite); hureaulite and vivianite (± ludlamite) in cleavage planes and around the triphylite grains (Fig. 2a)
Joc-4	I	Fap	Rare dendritic fluorapatite + albite + quartz (± muscovite), with erratic spessartine garnet rims
Joc-8	I	Trp ± viv ± lud ± fap	Dendritic triphylite + albite + quartz (± muscovite) altered by vivianite and ludlamite; apatite in albite + quartz between the triphylite dendrites
Joc-10a	I	Trp + viv ± hur ± barb ± fnd ± phosph ± fap ± lips	Dendritic triphylite + spessartine; vivianite in triphylite cleavage planes and at the boundary of triphylite and spessartine. Hureaulite and barbosalite (lipscombite) only in a small part of the thin section and replaced by frondelite and phosphosiderite (Figs. 2b, 2e, 2f)
Joc-10b	I	Trp+ hur + barb ± viv ± fnd ± phosph ± " jahn-(MnMnFe^{2+})"	Dendritic triphylite + spessartine + albite + quartz; hureaulite and barbosalite, and minor vivianite (only in one part of the thin section) in the triphylite cleavage planes. " jahnsite-(MnMnFe^{2+})" and frondelite as interganular grains between cleavelandite lamellae or frondelite as replacement phase of barbosalite; Phosphosiderite replaces frondelite.
Joc-12	I	Trp + fap + undetermined secondary Fe-Mn bearing phosphate	Rim of triphylite + quartz around spessartine. Fluorapatite in spessartine cracks. (Fig. 2c)
PS-071	II	Trp + viv	Massive triphylite; vivianite in cleavage planes and around triphylite grains
Joc-2	II	Rock-fnd ± phosph ± hur ± "ap" ± greifen	Massive fibroradial rockbridgeite-frondelite with hureaulite and apatite relics, replaced by phosphosiderite (± greifensteinite)
Joc-5	II	Trp	Unaltered massive triphylite
Joc-6	II	Trp	Unaltered massive triphylite
Joc-7	II	Trp + fsk + het + bar + hur+ jahn-(MnMnMn) + rock-fnd ± phosph ± leuco ± tav ± viv	Phosphate nodule of "olivine type phosphates", showing a concentric structure: - triphylite core; vivianite (only present in the centre of the core), and hureaulite, barbosalite (often replaced by frondelite-rockbridgeite) and tavorite in the cleavage planes of triphylite (Fig. 3b) - thin layer of ferrisicklerite around triphylite core; jahnsite (sometimes replaced by frondelite) in ferrisicklerite cleavage planes - layer of heterosite; patches of phosphosiderite and leucophosphite on heterosite; Mn-Fe-bearing oxides in heterosite cleavage planes - last layer of Mn-Fe-bearing oxides
Joc-9	II	Trp + hur + fnd ± viv	Massive triphylite altered by hureaulite (± vivianite). Frondelite in cavities, in triphylite cracks or on vivianite.
Joc-11	II	Trp+ fsk + het + barb + hur + jahn-(MnMnMn) + rock-fnd ± frst ± phosph ± tav ± viv ± leuco	Phosphate nodule of "olivine type phosphates", showing a concentric structure (Figs. 3a,c,d): - triphylite core; vivianite (only present in the centre of the core), and hureaulite, barbosalite (often replaced by frondelite-rockbridgeite) and tavorite in triphylite cleavage planes (Fig. 3a) - thin layer of ferrisicklerite around the triphylite core; jahnsite (sometimes replaced by frondelite) in ferrisicklerite cleavage planes (Fig. 3c) - thin layer of heterosite, ferristrunzite in its cleavage planes (Fig. 3d). Patches of phosphosiderite and leucophosphite on heterosite - last layer of Mn-Fe-bearing oxides
Joc-14	II	Trp + hur + undefined Fe-Mn bearing phosphate	Massive triphylite mainly altered by hureaulite
Joc-13a	III	Het + beu + fnd + lips + hur + tav + rob + phosph ± har	Exsolution lamellae of heterosite in beusite; hureaulite, tavorite and robertsite replace beusite; an intimate mixture of several secondary Fe-Mn-bearing phosphates and oxides form the external part. Spessartine rims this part of the nodule (Fig. 4a)
Joc-13b	III	Fsk + het + beu + hur + mit + tav	Exsolution lamellae of ferrisicklerite and heterosite in beusite; hureaulite, tavorite and mitridatite replace beusite (Fig. 4b)
Joc-13c	III	Fsk + het + beu + fap + hur + rob-mit+ tav± Stan ± har	Exsolution lamellae of heterosite in beusite; hureaulite, tavorite and mitridatite-robertsite replace beusite. Spessartine rims this part of the nodule, and also occurs between two lamellae of heterosite. Harrisonite is enclosed in spessartine (Fig. 4c)

T a = type assemblage, trp = triphylite, viv = vivianite, hur = hureaulite; fap = fluorapatite, rock = rockbridgeite, fnd = frondelite, jahn = jahnsite, whit = whiteite, phosph = phosphosiderite, "ap" = apatite group mineral; greifen = greifensteinite, lud = ludlamite, fsk = ferrisicklerite, het = heterosite, barb = barbosalite, leuco = leucophosphite, tav = tavorite, lips = lipscombite, frst = ferristrunzite, beu = beusite, rob = robertsite, mit = mitridatite, stan = staněkite, har = harrisonite

In the following description, primary (triphylite, beusite, and apatite), high-temperature hydrothermal (ferrisicklerite-heterosite and staněkite), and low-temperature hydrothermal phosphate minerals (hureaulite, barbosalite-lipscombite, tavorite, rockbridgeite-frondelite, and minerals of the jahnsite group) are successively described. To simplify the mineralogical descriptions, phosphate minerals produced by meteoric alteration are not described herein; however, their electron-microprobe compositions are available from the Depository (see above).

Triphylite

Triphylite from association I forms skeletal intergrowths with saccharoidal albite and quartz, and exhibits its typical greenish color, which turns bluish if it is largely replaced by vivianite (Fig. 2a). In association II, triphylite is massive and shows a darker greenish color; in association III, triphylite is absent but its alteration products (ferrisicklerite and heterosite) occur as lamellae in beusite (see below). Under the microscope, triphylite is similar in the two associations and appears as a non-pleochroic translucent to light grey mineral. In association I, triphylite may be relatively fresh (unaltered) or almost completely replaced by vivianite, hureaulite (Figs. 2a, 2d), or ludlamite. Hureaulite can occasionally be associated with deep greenish barbosalite. These replacements occur along the two cleavage planes of triphylite and isolate subrectangular grains of unaltered triphylite, producing a cellular texture (Fig. 2d). In association I, triphylite may also form polycrystalline intergrowths with garnet, quartz, and apatite (Fig. 2b); the latter generally crystallizes in the matrix, in contact with triphylite crystals, or in cracks in garnet (Fig. 2c). Triphylite can also enclose isolated grains of garnet associated with quartz (Fig. 2e), or form a rim (±200 μm in width) between this garnet and the albite + quartz + muscovite (± microcline) matrix (Fig. 2c); garnet may also crystallize on the border of triphylite (±100 μm in width; Fig. 2f). This mineral association is intensively fractured and the cracks are filled with chamosite in garnet and with vivianite in triphylite (Figs. 2b, e). Hureaulite doesn't replace triphylite occurring with the garnet intergrowths, but vivianite occurs at grain boundaries between the different minerals (Fig. 2b). Some isolated grains of triphylite can also be enclosed in the garnet. In sample Joc-12, several rims occur on the border of garnet grains; these rims are composed of quartz and/or triphylite.

In association II, hureaulite and barbosalite replace triphylite along cleavage planes (Fig. 3a) and are often associated with yellowish polygranular tavorite (Fig. 3b). Moreover, triphylite oxidizes progressively into ferrisicklerite and heterosite following the so-called "Quensel-Mason" sequence: $Li(Fe^{2+},Mn^{2+})PO_4$ – $Li_{1-x}(Fe^{3+},Mn^{2+})PO_4$ – $(Fe^{3+},Mn^{3+})PO_4$ (Quensel 1937, Mason 1941). The optical orientation of the three minerals is preserved during this oxidation (Figs. 3a, c, d). It is noteworthy that the replacement of triphylite by hureaulite + barbosalite (± tavorite) becomes more and more intense when approaching the contact between triphylite and ferrisicklerite (Figs. 3a, c).

Representative chemical compositions of triphylite minerals from associations I and II are given in Table 3.Triphylite from the two associations has a similar composition and shows a high lithiophilite component (0.42% and 0.44% of lithiophilite in triphylite from associations I and II, respectively). In sample Joc-14 from association II, this lithiophilite component is higher and reaches 0.49%. Lower MgO and SiO_2 contents are also observed in triphylite from this sample as the $Mg/(Fe_{tot}+Mn_{tot}+Mg)$ ratio only reaches 0.005, while it rises to 0.016 in other triphylites from association II and the SiO_2 wt.% drops to 0.00, whereas it is always approximately 0.25% (0.20–0.27) in triphylite from association I and II. It is noteworthy that triphylite from association I which is associated with garnet has a higher $Mg/(Fe_{tot}+Mn_{tot}+Mg)$ ratio (0.026) compared to the other triphylite from the same association (0.017).

Beusite

Reddish flesh-colored beusite only occurs in association III, where it forms intergrowths with lamellae of brownish ferrisicklerite and purplish heterosite (Fig. 4). Phosphate minerals from this association are intensively fractured by veinlets which occur approximately perpendicular to the lamellae (Fig. 4a) and are generally filled with Mn-Fe-bearing oxide minerals and/or deep reddish robertsite. Beusite is replaced by an intimate mixture of pleochroic hureaulite (colorless to deep orange) and greenish to yellowish tavorite. Minerals from the mitridatite-robertsite series, and more rarely phosphosiderite, commonly cover the hureaulite and tavorite (Fig. 4b). This replacement of beusite generally takes place in contact with the lamellae, and is rarely extended into these lamellae (Fig. 4b). The alteration is more important near the cracks and on the border of this nodule (Fig. 4c). On this border, small grains of barbosalite crystallize with hureaulite and tavorite, and Mn-Fe oxide minerals are more abundant, hiding the previous existing minerals. Acicular orange frondelite, bluish phosphosiderite, and whitish leucophosphite may also appear in this part of the sample (Fig. 4c). As was mentioned above, it is quite rare to observe intergrowths of triphylite in beusite; such an association has only been observed in the Sidenjsö dike, in the Stora Persholmen pegmatite in Sweden (Smeds *et al.* 1998), and in the Yellowknife pegmatite field in Canada (Wise & Černý 1990). Nevertheless, at these three localities, the Mn# [Mn/(Mn+Fe)] of beusite-graftonite attains 0.571, 0.534, and 0.552, respectively, which is not far from the 50% boundary. Our electron-microprobe data

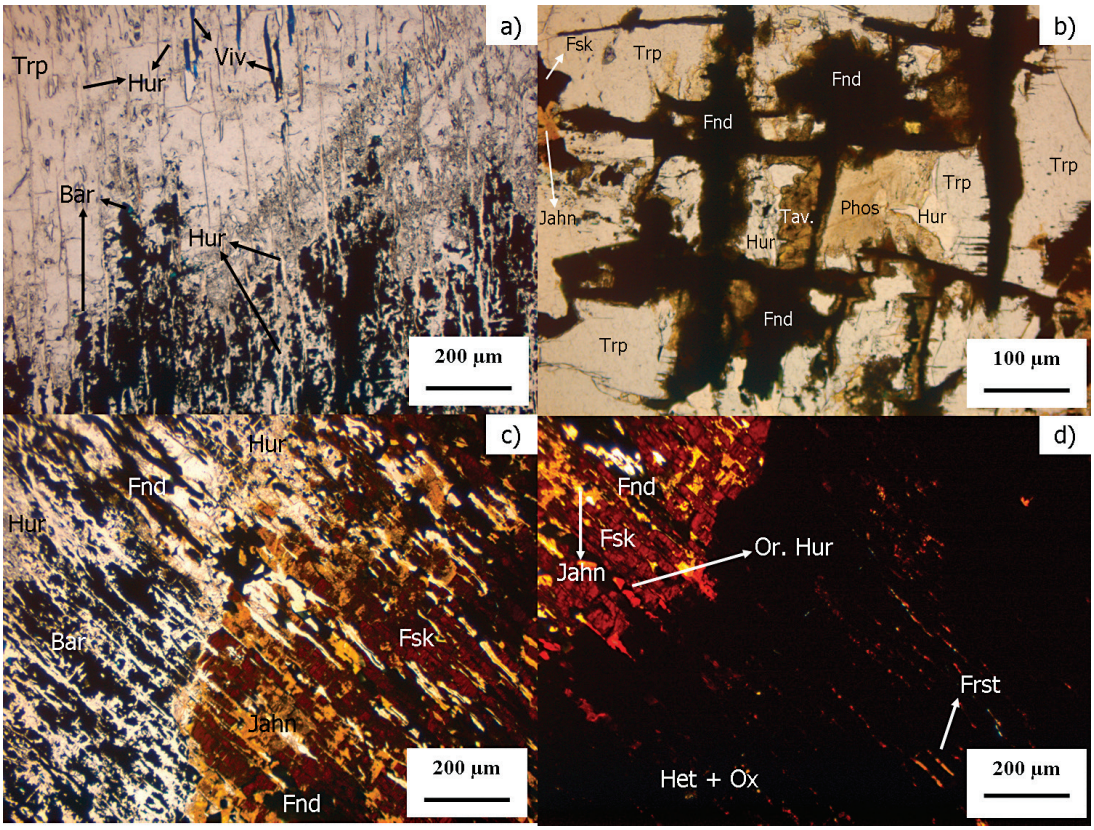

FIG. 3. Phosphate minerals from association II: progressive topotatic oxidation of triphylite in ferrisicklerite and finally in heterosite, with their own alteration minerals (a,c,d) (a) Cellular texture in triphylite (Trp). The latter is replaced along its perpendicular cleavage planes by colorless hureaulite (Hur) and vivianite (Viv), in the upper part of the picture, and then by colorless hureaulite and deep green barbosalite (Bar), at the bottom of the picture, near the contact between triphylite and ferrisicklerite. Association II, Joc-11, plane-polarized light. (b) Cellular texture in triphylite. The latter is replaced by hureaulite, barbosalite that is oxidized to dark frondelite (Fnd), and tavorite (Tav). On the left side, triphylite is oxidized to ferrisicklerite (Fsk), which is altered by jahnsite (Jahn). Phosphosiderite (Phos) later replaces hureaulite. Association II, Joc-7, plane-polarized light (c) Oxidation of triphylite to ferrisicklerite (Fsk). The optical orientation is preserved. Yellow jahnsite and dark non-pleochroic frondelite (Fnd) replaces ferrisicklerite along its cleavage planes. This dark frondelite also replaces barbosalite in triphylite. Association II, Joc-11, plane-polarized light. (d) Oxidation of ferrisicklerite to heterosite (Het). Orange hureaulite (Or. Hur) appears in the cleavage planes of ferrisicklerite and oxide minerals (ox) and yellow ferristrunzite (frst) in the cleavage planes of heterosite. Association II, Joc-11, plane-polarized light.

shows that the Mn# of beusite from Jocão is similar to that of beusite from the Sidenjsö dike, 0.569 (Table 3, Fig. 4). However the Ca content of beusite from this dike is much lower (0.345 Ca *pfu*) than the Ca content of beusite from Jocão (0.559 Ca *pfu*). A higher Ca content has been observed in beusite from Yellowknife; it corresponds to 0.943 Ca *pfu* (Wise & Černý 1990).

Apatite

Greenish apatite is common in association I, where it forms intergrowths with reddish garnet and triphylite. It can also appear as greenish crystals in albite. Apatite was not observed macroscopically in association III, but under the microscope, we found this phosphate as small intergrowths or isolated grains in heterosite lamellae, or associated with garnet between two lamellae of heterosite (Fig. 4d). In association I, under the microscope, this mineral appears as small idiomorphic hexagonal crystals (less than 100 µm wide) or larger anhedral masses, in the albite ± quartz matrix; at the contact with one or several grains of triphylite in albite (± quartz); as intergrowths with garnet and triphylite; and completely enclosed in garnet, or appearing in cracks within garnet

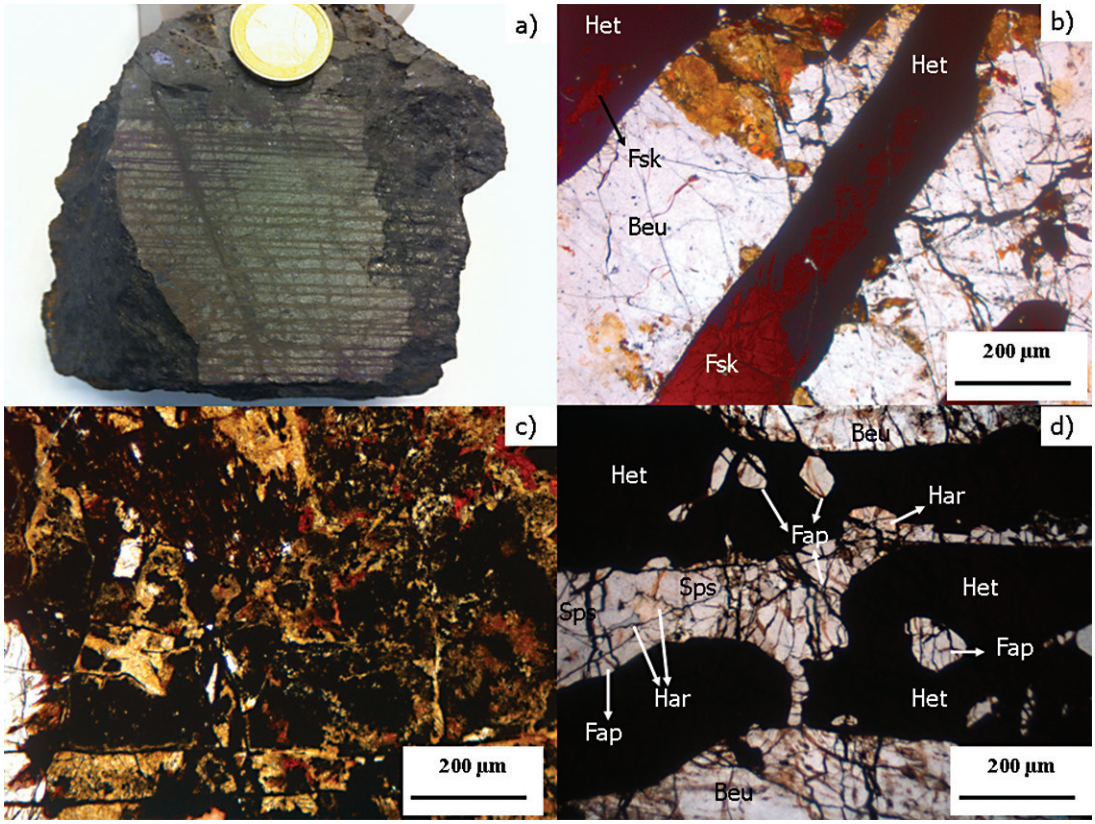

FIG. 4. Phosphate minerals of association III. (a) Sample Joc-13 showing lamellae of ferrisicklerite (dark brown) and heterosite (purplish) in beusite. It is noteworthy that the ferrisicklerite lamellae are mainly located in the center part of this sample, while the heterosite lamellae mainly occur at the border. The upper side (both sides of the coin) constitute a darker oxidized border, wherein the blue color corresponds to phosphosiderite. (b) Orange ferrisicklerite (Fsk) lamellae partially oxidized to purple heterosite (Het) occurring in beusite (Beu). Orange hureaulite and tavorite appear in the beusite, and are generally replaced by yellow to orange minerals from the mitridatite-robertsite series. All these minerals generally form an intimate yellowish mixture (between the two lamellae). This replacement does not affect the lamellae. Association III, Joc-13b, plane-polarized light. (c) Oxidized border of the nodule wherein beusite and the lamellae are completely replaced by phosphate minerals, principally members of the mitridatite-robertsite series, but also frondelite, leucophosphite, and phosphosiderite, and by (Mn, Fe)-bearing oxide minerals. Association III, Joc 13a, plane-polarized light. (d) Association of fluorapatite (Fap), spessartine garnet (Sps), and harrisonite (Har) between two heterosite lamellae in beusite. Fluorapatite may also be completely enclosed in heterosite lamellae. Association III, Joc-13c, crossed polars.

(Fig. 2c). Apatite sometimes exhibits a light greenish color under the microscope.

Representative electron-microprobe analyses show that all apatite corresponds to fluorapatite, except for a very small grain occurring in hureaulite from sample Joc-2, which shows a composition exactly halfway between fluorapatite and hydroxylapatite (Table 4). Fluorapatite from association I has MnO contents of 1.08 to 8.50 wt.% MnO. Fluorapatite from association III, which occurs in the heterosite lamellae, is quite depleted in F (2.38 wt.% F) and enriched in MnO (11.73 wt.% MnO) compared to those of association I (Table 4).

Ferrisicklerite and heterosite

Ferrisicklerite and heterosite crystallize within the nodules of associations II and III. In association II, all minerals of the "Quensel-Mason" sequence are generally observed (Fig. 3): triphylite is oxidized in ferrisicklerite, and then ferrisicklerite is oxidized in heterosite. Triphylite constitutes the massive core of the elliptic nodules, which may reach 10 cm in diameter

(Joc-7). Ferrisicklerite then forms a first concentric layer around triphylite, and heterosite a second layer around ferrisicklerite. Between triphylite and ferrisicklerite, an intermediate layer constituted by hureaulite and barbosalite frequently occurs (Fig. 3a, c). The external layer of this concentric structure is composed of late Mn-Fe oxide minerals. The triphylite core constitutes the main volume of the nodule, and ferrisicklerite occurs as a thin layer. These three minerals have the same optical orientation, and are replaced by several secondary phos-

TABLE 3. CHEMICAL COMPOSITION OF QUENSEL-MASON SEQUENCE MINERALS, BEUSITE AND STANĚCKITE, FROM JOCÃO PEGMATITE, MINAS GERAIS, BRAZIL

Mineral	Trp	Trp	Trp	Trp	Trp	Beu	Fsk	Fsk	Fsk	Het	Het	Het		Stan	Stan
Samples	a	b	c	d	e	f	g	h	i	j	k	l		m	n
Association	I	I	I	II	II	III	II	III	III	II	III	III		III	III
Number of analyses	28	18	10	49	8	17	15	7	6	14	17	4		6	2
SiO_2 wt.%	0.23	0.22	0.27	0.20	0.00	0.00	0.27	0.24	0.95	0.25	0.03	1.06	SiO_2 wt.%	0.00	0.01
P_2O_5	45.62	45.54	45.65	45.78	46.56	41.69	46.30	46.83	45.14	46.14	47.32	45.34	P_2O_5	32.66	33.62
Al_2O_3	0.00	0.00	0.00	0.00	0.00	0.00	0.00	0.00	0.00	0.00	0.00	0.00	Al_2O_3	0.00	0.00
Fe_2O_3*	0.08	-	0.03	0.27	0.41	0.63	29.72	29.54	31.06	30.23	28.74	30.90	Fe_2O_3*	35.76	38.44
FeO*	26.15	26.53	25.87	25.53	23.56	21.15	-	-	-	-	-	-	FeO*	2.36	-
MgO	0.60	0.70	0.46	0.42	0.14	0.31	0.46	0.89	0.83	0.46	0.92	0.79	MgO	0.86	0.85
Mn_2O_3*	-	-	-	-	-	-	-	-	-	17.59	20.28	14.69	Mn_2O_3*	-	4.12
MnO*	19.66	19.29	20.04	20.17	22.45	29.00	20.51	21.22	20.61	4.39	3.27	7.75	MnO*	29.32	24.90
ZnO	0.09	0.06	0.13	0.05	0.07	0.29	0.09	0.02	0.09	0.07	0.10	0.11	ZnO	0.61	0.67
CaO	0.03	0.02	0.04	0.02	0.10	9.21	0.10	0.11	0.14	0.31	0.22	0.21	CaO	0.21	0.22
Na_2O	0.00	0.00	0.00	0.00	0.00	0.00	0.00	0.00	0.00	0.00	0.00	0.00	Na_2O	0.00	0.00
Li_2O*	9.36	9.27	9.47	9.50	9.72	-	3.74	3.56	2.60	0.00	0.03	-	K_2O	0.00	0.00
K_2O	0.00	0.00	0.00	0.00	0.01	0.00	0.04	0.01	0.02	0.14	0.09	0.01	F	0.53	0.75
													O≡F	-0.22	-0.32
Total	101.82	101.63	101.96	101.94	103.01	102.28	101.23	102.42	101.44	99.58	101.00	100.85			
													Total	102.09	103.26
Si *apfu*	0.004	0.006	0.007	0.005	0.000	0.000	0.007	0.006	0.024	0.006	0.001	0.027			
P	0.996	0.994	0.993	0.995	1.000	2.000	0.993	0.994	0.976	0.994	0.999	0.973	Si *apfu*	0.000	0.000
Al	0.000	0.000	0.000	0.000	0.000	0.000	0.000	0.000	0.000	0.000	0.000	0.000	P	1.000	1.000
Fe^{3+}	0.001	0.000	0.001	0.005	0.008	0.027	0.567	0.557	0.597	0.579	0.539	0.589	Al	0.000	0.000
Fe^{2+}	0.563	0.572	0.556	0.548	0.500	1.002	-	-	-	-	-	-	Fe^{3+}	0.973	1.016
Mg	0.023	0.027	0.018	0.016	0.005	0.026	0.017	0.033	0.032	0.018	0.034	0.030	Fe^{2+}	0.072	-
Mn^{3+}	-	-	-	-	-	-	-	-	-	0.340	0.385	0.283	Mg	0.046	0.045
Mn^{2+}	0.429	0.421	0.436	0.439	0.483	1.392	0.440	0.451	0.446	0.095	0.070	0.167	Mn^{3+}	-	0.110
Zn	0.002	0.001	0.002	0.001	0.001	0.012	0.002	0.000	0.002	0.001	0.002	0.002	Mn^{2+}	0.898	0.741
Ca	0.001	0.000	0.001	0.001	0.003	0.559	0.003	0.003	0.004	0.008	0.006	0.006	Zn	0.016	0.017
Na	0.000	0.000	0.000	0.000	0.000	0.000	0.000	0.000	0.000	0.000	0.000	0.000	Ca	0.008	0.008
Li	0.968	0.962	0.979	0.981	0.992	-	0.381	0.358	0.265	0.000	0.003	-	Na	0.000	0.000
K	0.000	0.000	0.000	0.000	0.000	0.000	0.001	0.000	0.001	0.005	0.003	0.000	K	0.000	0.000
Σ M	1.983	1.983	1.993	1.996	1.992	3.018	1.411	1.396	1.347	1.046	1.042	1.077	F	0.061	0.083
$Fe_{tot}/(Fe_{tot}+Mn_{tot})$	0.568	0.576	0.561	0.557	0.513	0.425	0.563	0.553	0.572	0.571	0.542	0.567		0.537	0.544
$Fe_{tot}/(Fe_{tot}+Mn_{tot}+Mg)$	0.555	0.561	0.551	0.549	0.510	0.421	0.553	0.535	0.556	0.561	0.525	0.551		0.525	0.531
$Mg/(Fe_{tot}+Mn_{tot}+Mg)$	0.023	0.026	0.017	0.016	0.005	0.011	0.017	0.032	0.029	0.017	0.033	0.028		0.023	0.024
$Mn/(Fe_{tot}+Mn_{tot}+Mg)$	0.422	0.413	0.432	0.435	0.485	0.569	0.430	0.433	0.415	0.422	0.442	0.421		0.451	0.445

- : not determined

Number of cations was calculated on the basis of 1 (P+Si) per formula unit (*pfu*) for triphylite (Trp), ferrisicklerite (Fsk), heterosite (Het), and staněkite (Stan) and on the basis of 2 (P+Si) *pfu* for beusite (Beu); * In triphylite, Li and Fe^{3+} are calculated to maintain the charge balance and to have no excess in Li on M1 site of triphylite. In ferrisicklerite and heterosite, all Fe is assumed to be ferric and Li, Mn^{2+}, and Mn^{3+} were calculated to maintain charge balance. In beusite, Fe^{3+} is calculated to maintain the charge balance
a = Triphylite, assemblage I, samples Joc-3, 8, 10, 12; b = triphylite associated with garnet, assemblage I, samples Joc-10, 12 ; c = triphylite without garnet, assemblage I, samples Joc-3, 8; d = triphylite, assemblage II, samples Joc-5, 7, 9, 11 ; e = Fe-poorer and Mn-richer triphylite, assemblage II, sample Joc-14 ; f = beusite assemblage III, samples Joc-13c ; g = ferrisicklerite, assemblage II, samples Joc-7, Joc-11 ; h = Si-poor ferrisicklerite, assemblage III, samples Joc-13 ; i = Si-rich ferrisicklerite, samples Joc-13 ; j = heterosite, assemblage II, samples Joc-7, Joc-11 ; k = Si-poor heterosite, assemblage III, samples Joc-13 ; l = Si-rich heterosite, assemblage III, samples Joc-13; m = Mn^{3+}- free staněkite, assemblage III, Joc-13c; n = Mn^{3+}- bearing staněkite.

phate minerals along their cleavage planes, producing a cellular texture similar to that observed in triphylite (Figs. 2d, 3b). It is noteworthy that the secondary phosphate associations, occurring in the cleavage planes of ferrisicklerite and heterosite, are significantly different from each other: the cleavage planes of ferriscklerite are filled with yellowish jahnsite, dark acicular minerals from the frondelite-rockbridgeite series, and minor pleochroic hureaulite (colorless to deep orange) (Fig. 3c, d), whereas the cleavage planes of heterosite are filled with Mn-Fe oxide minerals and ferristrunzite (Fig. 3d). When they occur as alteration products, white

TABLE 4. CHEMICAL COMPOSITION OF FLUORAPATITE (FAP), "APATITE" (AP), HUREAULITE (HUR), BARBOSALITE (BAR), LIPSCOMBITE (LIP), AND TAVORITE (TAV) FROM THE JOCÃO PEGMATITE, MINAS GERAIS, BRAZIL

Mineral	Fap	Ap	Fap	Hur	Hur	Hur	Hur	Hur	Hur	Hur	Hur	Hur	Bar	Bar	Lip	Tav	Tav
Samples	a	b	c	d	e	f	g	h	i	j	k	l	m	n	o	p	q
Association	I	I	III	I	I	I	II	II	II	III	III	III	I	II	I	II	III
Number of analyses	31	3	4	2	4	4	10	8	6	7	2	2	4	6	4	3	16
SiO_2 (wt.%)	0.00	0.00	0.00	0.00	0.00	0.00	0.00	0.00	0.00	0.00	0.00	0.00	0.00	0.00	0.00	0.00	0.00
P_2O_5	42.05	41.92	41.94	39.41	39.08	38.66	39.38	39.53	39.71	40.03	39.15	40.26	36.88	36.83	36.45	41.23	42.45
Al_2O_3	0.00	0.00	0.00	0.00	0.00	0.00	0.00	0.00	0.00	0.00	0.00	0.00	0.26	0.01	0.00	0.00	0.01
Fe_2O_3*	-	-	-	0.70	-	-	-	-	-	-	-	4.15	44.36	42.71	44.70	46.02	44.99
FeO*	0.39	0.53	0.82	15.41	17.66	9.11	10.79	7.40	17.85	4.73	16.13	12.79	12.31	13.65	11.28	-	-
MgO	0.01	0.00	0.01	0.08	0.35	0.23	0.62	0.63	0.96	0.08	0.07	0.08	0.03	0.29	0.02	0.10	0.07
MnO	5.31	3.72	11.73	32.49	30.25	39.92	36.64	40.80	30.27	42.58	29.95	28.51	1.77	2.56	2.01	0.55	2.47
ZnO	0.01	0.05	0.02	0.08	0.06	0.14	0.08	0.07	0.09	0.55	0.41	0.33	0.05	0.11	0.08	0.02	0.05
CaO	50.23	50.96	44.75	0.30	0.84	0.73	0.97	0.65	0.57	3.17	2.63	2.52	0.02	0.02	0.03	0.01	0.10
Na_2O	0.00	0.00	0.00	0.00	0.00	0.00	0.00	0.00	0.00	0.00	0.00	0.00	0.00	0.00	0.00	0.00	0.05
K_2O	0.00	0.00	0.00	0.00	0.01	0.00	0.14	0.00	0.00	0.00	0.01	0.01	0.03	0.02	0.02	0.01	0.07
Li_2O	-	-	-	-	-	-	-	-	-	-	-	-	-	-	-	8.55	9.28
H_2O**	0.00	0.89	0.65	12.50	12.40	12.27	12.64	12.73	12.80	13.18	12.63	12.78	4.68	4.67	4.63	5.23	6.90
F	4.84	1.87	2.38	-	-	-	-	-	-	-	-	-	-	-	-	-	-
O≡F	-2.04	-0.79	-1.00	-	-	-	-	-	-	-	-	-	-	-	-	-	-
Total	100.79	99.15	101.3	100.97	100.65	101.06	101.26	101.82	102.25	104.32	100.98	101.43	100.39	100.87	99.22	101.72	104.93
Si *apfu*	0.000	0.000	0.000	0.000	0.000	0.000	0.000	0.001	0.000	0.000	0.000	0.000	0.000	0.000	0.000	0.000	0.000
P	3.000	3.000	3.000	4.000	4.000	4.000	4.000	3.999	4.000	4.000	4.000	4.000	2.000	2.000	2.000	1.000	1.000
Al	0.000	0.000	0.000	0.000	0.000	0.000	0.000	0.000	0.000	0.000	0.000	0.000	0.020	0.001	0.000	0.000	0.000
Fe^{3+}	-	-	-	0.063	-	-	-	-	-	-	-	0.367	2.135	2.061	2.083	0.992	0.942
Fe^{2+}	0.028	0.037	0.058	1.545	1.787	0.931	1.084	0.740	1.777	0.467	1.628	1.256	0.664	0.734	0.728	-	-
Mg	0.001	0.001	0.001	0.014	0.062	0.041	0.109	0.112	0.170	0.014	0.012	0.014	0.020	0.028	0.002	0.004	0.003
Mn^{2+}	0.380	0.267	0.840	3.300	3.097	4.133	3.723	4.131	3.050	4.257	3.062	2.834	0.095	0.138	0.139	0.013	0.059
Zn	0.001	0.003	0.001	0.007	0.005	0.013	0.007	0.006	0.007	0.048	0.036	0.028	0.002	0.005	0.003	0.000	0.000
Ca	4.535	4.616	4.051	0.039	0.109	0.096	0.124	0.083	0.073	0.401	0.340	0.316	0.001	0.001	0.002	0.000	0.003
Na	0.000	0.000	0.000	0.000	0.000	0.000	0.000	0.000	0.000	0.000	0.000	0.000	0.000	0.000	0.000	0.000	0.003
K	0.000	0.000	0.000	0.000	0.001	0.000	0.021	0.000	0.000	0.000	0.001	0.002	0.002	0.002	0.003	0.000	0.002
Li	-	-	-	-	-	-	-	-	-	-	-	-	-	-	-	0.986	1.037
F	1.291	0.500	0.635	-	-	-	-	-									
OH	0.000	0.500	0.065	2.000	-	-	2.116	2.144	2.157	2.373	2.162	2.000	2.000	2.000	2.000	1.000	1.000
$Fe_{tot}/(Fe_{tot}+Mn_{tot})$	-	-	-	0.328	0.366	0.183	0.226	0.152	0.368	0.099	0.347	0.364	0.967	0.953	0.953	0.987	0.941

- : not determined

Number of cations was calculated on the basis of 3 (P+Si) per formula unit (*pfu*) for minerals of apatite group, on the basis of 4 (P+Si) *pfu* for hureaulite; on the basis of 2 (P+Si) *pfu* for barbosalite and lipscombite; and on the basis of 1 (P+Si) *pfu* for tavorite; * Fe^{3+} is calculated to maintain the charge balance; ** H_2O content was calculated according to the ideal formulae.

a = Fluorapatite, assemblage I (without sample Joc-2), samples Joc-1, 3, 4, 8, 10, 12; b = "apatite", assemblage I, sample Joc-2; c = Fluorapatite, assemblage III, sample Joc-13; d = Fe^{3+}-bearing and Fe-rich hureaulite, assemblage I, samples Joc-3, 10a, 10b; e = Fe^{2+}-rich hureaulite, assemblage I, samples Joc-10a, 10b ; f = hureaulite, assemblage I, Joc-2; g = pleochroic hureaulite, assemblage II, samples Joc-7, Joc-11 ; h = colourless hureaulite, assemblage II, samples Joc-7, Joc-9, Joc-11 ; i = colorless hureaulite, assemblage II, sample Joc-14; j = pleochroic hureaulite, assemblage III, sample Joc-13; k = pleochroic Fe^{2+}-rich hureaulite, assemblage III, sample Joc-13a, l = pleochroic Fe-rich, Fe^{3+}-bearing hureaulite, assemblage III, sample Joc-13a; m = barbosalite, assemblage I, sample Joc-10a; n = barbosalite, assemblage II, samples Joc-7, Joc-11; o = lipscombite, assemblage I, Joc-10a; p = Tavorite, assemblage II, Joc-7, Joc-11; q = tavorite, assemblage III, Joc-13a, 13b.

leucophosphite and/or colorless phosphosiderite don't appear in the cleavage planes, but crystallize as spots (400 μm diameter) in ferrisicklerite and heterosite, overprinting the former cellular texture.

In association III, ferrisicklerite and heterosite appear as thin lamellae reaching several centimeters in length, included in massive beusite (Fig. 4a). Within a single lamella, ferrisicklerite may be oxidized to heterosite (Fig. 4b). The contact between these two minerals is sharp, and the oxidation process seems to be more intense on the border of the lamellae (Fig. 4b). The oxidation is also more pronounced on the border of the phosphate nodule, where most of the lamellae have been completely replaced by heterosite (Fig. 4a). At the rim of the nodule, the intergrowth textures are progressively hidden by secondary phosphate minerals, like barbosalite, hureaulite, tavorite, frondelite, leucophosphite, phosphosiderite, and by Fe-Mn oxide minerals (Fig. 4c). Ferrisicklerite and heterosite lamellae from the core of the nodule remain relatively unaltered, and are only crosscut by veinlets of oxide minerals and robertstite. When the alteration is more pronounced, beusite progressively transforms into a hureaulite + tavorite intergrowth, whereas the heterosite lamellae remain unaffected (Fig. 4b). Late mitridatite, robertsite, and phosphosiderite then progressively replace the hureaulite + tavorite association, and crosscut heterosite and beusite lamellae (Fig. 4b). Leucophosphite occurs as white spots (400 μm) in the heterosite lamellae or at the junction between beusite and heterosite.

Representative electron-microprobe data for ferrisicklerite and heterosite of association II show that their Mg-Fe_{tot}-Mn_{tot} contents are similar to those of triphylite from the same association (Table 3). This observation is in good agreement with the preservation of the Mg-Fe_{tot}-Mn_{tot} contents in phosphate minerals of the "Quensel-Mason" sequence (Fransolet *et al.* 1985, 1986, Baijot *et al.* 2012). Finally, it is noteworthy that a significant amount of Mn^{2+}, up to 7.75 wt.% MnO (0.167 Mn^{2+} *pfu*), remains in some heterosite samples (Table 3), while this element is generally considered as completely oxidized in this mineral. This observation is in good agreement with Hatert *et al.* (2011), who investigated olivine-type phosphate minerals by secondary ion mass spectrometry (SIMS) to determine their Li contents, and showed that heterosite from Ariakas, Namibia, contains 0.05 Mn^{2+} *pfu*.

Staněkite

Staněkite occurs in sample Joc-13c from association III, in close association with heterosite lamellae. It appears as anhedral opaque grains in contact with heterosite and beusite, which, unlike the (Fe-Mn)-oxide minerals, are not especially developed in the cleavage planes of heterosite. As shown in Table 3, it is sometimes necessary to consider a significant amount of Mn^{3+} to maintain charge balance, leading to the empirical formula: $(Fe^{3+}_{1.02}Mn^{2+}_{0.74}Mn^{3+}_{0.11}Mg_{0.05}Zn_{0.02}Ca_{0.01})_{\Sigma 1.95}(PO_4)(O_{1.96}F_{0.08})$. This formula shows a solid solution towards joosteite, $Mn^{2+}(Mn^{3+}, Fe^{3+})(PO_4)O$, the Mn^{3+}-bearing analogue of staněkite (Keller *et al.* 2007).

Hureaulite

In association I, some dendritic crystals of triphylite appearing in the albite ± quartz matrix are partially or completely replaced by salmon pink hureaulite. In association II, pinkish crystals up to 2 cm in length are perched on greenish frondelite or crystallize in massive triphylite of the nodule core. In hand specimen, hureaulite is difficult to identify in association III.

Under the polarizing microscope, the replacement of triphylite by hureaulite occurs along the cleavage planes of triphylite in associations I and II (Figs. 2d and 3a, respectively). In association I, colorless hureaulite is mainly associated with blue vivianite (Fig. 2d) and may partially or completely replace dendritic triphylite, producing a dendritic association of hureaulite and albite. In this case (Joc-10a), hureaulite is also associated with greenish barbosalite and reddish to brownish lipscombite, and may be replaced by mauve fibroradial crystals of phosphosiderite. In association II, massive triphylite is also replaced by hureaulite and vivianite along its cleavage planes (Fig. 3a), but close to the contact between triphylite and ferrisicklerite, triphylite is completely replaced by hureaulite and by bottle green barbosalite (Fig. 3c). Tavorite may be present in association with hureaulite and barbosalite but is relatively less abundant; leucophosphite and phosphosiderite replace hureaulite crystals (Fig. 3b). Hureaulite is slightly pleochroic (colorless to light yellow) near the contact between altered triphylite and ferrisicklerite, and becomes strongly pleochroic (light yellow to orange) in the cleavage planes of ferrisicklerite, where it is associated with minerals of the jahnsite group and of the rockbridgeite-frondelite series (Fig. 3c, 3d).

Electron-microprobe compositions of hureaulite show significant variations of the Fe and Mn contents for different samples collected from the Jocão pegmatite, but also for different grains occurring in the same sample (Table 4). For example, in sample Joc-7, strongly pleochroic hureaulite contains *ca.* 8–16 wt.% FeO; slightly pleochroic hureaulite associated with barbosalite, near the contact with ferrisicklerite, contains 7 wt.% FeO; and colorless non-pleochroic hureaulite, associated with barbosalite and replacing triphylite, only contains 3 wt.% FeO. Nevertheless, in Joc-11, the FeO content of colorless hureaulite, associated with barbosalite, varies from 3 to 10 wt.% FeO. Hureaulite from associations I and II, which are associated with vivianite, show higher FeO contents (*ca.* 11–21 wt.% FeO), compared to those associated with barbosalite (*ca.* 3–14 wt.% FeO) (Table 4). In

association III, hureaulite grains from the same sample exhibit strong variation in their Mn and Fe contents (Table 4); for example, hureaulite replaced by minerals of the midridatite-robertsite series is depleted in FeO (*ca*. 2–8 wt.% FeO), compared to those replaced by leucophosphite and phosphosiderite (16–17 wt.% FeO). Finally, hureaulite from association III clearly shows high CaO contents (*ca*. 2–5 wt.% CaO), compared to hureaulite samples from the other two associations (*ca*. 0–1 wt.% CaO) (Table 4).

A comparison between the electron-microprobe data and the optical properties of hureaulite shows the absence of correlation between the chemical composition and pleochroism, as previously observed in samples from the Sapucaia pegmatite (Baijot *et al*. 2012). As suggested by Fransolet (1976), a small amount of Fe^{3+} in hureaulite could explain its different tinges of pleochroism, but in Jocão, most of pleochroic hureaulite samples do not contain Fe^{3+}.

Barbosalite and lipscombite

Bottle-green barbosalite is associated with salmon-pink hureaulite in triphylite from associations I and II; however, it was not detected in association III. Under the polarizing microscope, barbosalite grains show nearly opaque cores, surrounded by a deep greenish blue rim, which is rarely pleochroic (olive green to deep greenish blue); barbosalite progressively invades the orthogonal cleavage planes of triphylite (Figs 3a, c). Polygranular yellowish tavorite generally crystallizes with barbosalite and hureaulite, but is relatively less abundant. In association II, where triphylite and ferrisicklerite occur, the replacement of triphylite by hureaulite and barbosalite (± tavorite) is more and more intense close to the contact between the two olivine-type minerals; rectangles of triphylite forming the cellular texture are finally completely replaced (Fig. 3a, c). In association II, barbosalite is sometimes partially or completely replaced by fibroradial crystals of rockbridgeite-frondelite (Fig. 3c). In association I, sample Joc-10a, a crystal of triphylite is partially replaced by reddish lipscombite, which is dimorphous with barbosalite; other parts of this triphylite crystal show the classical cellular texture with hureaulite and barbosalite. Phosphosiderite occasionally replaces lipscombite. Lipscombite also appears in association III, forming an intimate intergrowth with tavorite, frondelite, and Fe-Mn oxide minerals, in the oxidized rim of the nodule.

The chemical compositions of barbosalite and lipscombite from association I are similar to that of barbosalite from association II (Table 4). These minerals always contain small amounts of MnO (*ca*. 1–3 wt.% MnO); the larger observed variations concern Fe, which attains *ca*. 5–18 wt.% FeO and *ca*. 38–50 wt.% Fe_2O_3, corresponding to 0.26–1.06 Fe^{2+} *pfu* and 1.91–2.38 Fe^{3+} *pfu*, respectively. As previously observed in other pegmatites (Lindberg & Pecora 1954, 1955, Čech *et al*. 1961, Čech *et al*. 1972, Fransolet 1975, Baijot *et al*. 2012), barbosalite and lipscombite from Jocão show a deficit in $Fe^{2+}$and an excess in Fe^{3+} (Table 4); this feature is not surprising since lipscombite without Fe^{2+} has been synthesized by Gheith (1953). Moreover, some authors have agreed to consider an oxidation process in Fe^{2+}- and Fe^{3+}-bearing phosphate minerals (Moore 1971, Fransolet 1975, 1976, 2007, Moore 1982, Vignola *et al*. 2011, Baijot *et al*. 2012), which corresponds to the following substitution mechanism: $Fe^{2+} + OH^- \rightarrow Fe^{3+} + O^{2-} + 1/2\ H_2$ (Moore 1982, Fransolet, 1975, 2007, Baijot *et al*. 2012). In this case, we may admit the existence of a solid solution between $Fe^{2+}Fe^{3+}{}_2(PO_4)_2(OH)_2$ and $Fe^{3+}{}_3(PO_4)_2O(OH)$, and consider the formula $Fe^{2+}{}_{1-x}Fe^{3+}{}_{2+x}(PO_4)_2O_x(OH)_{2-x}$ for barbosalite and lipscombite. However, direct determinations of the water contents and/or of the Fe^{2+}/Fe^{3+} ratio of our samples would be necessary to confirm the occurrence of such a substitution mechanism; such experiments were not done because of the small size of the barbosalite and lipscombite grains and their intimate mixture with other phosphate minerals.

Tavorite

Tavorite was only recognized under the polarizing microscope in associations II and III, in which it appears as light yellowish-green grains frequently showing a polygranular texture under crossed polars. In association II, tavorite crystallizes in close association with barbosalite, frondelite *s.l.*, and hureaulite (Fig. 3b); in association III, tavorite occurs in the oxidized border of the nodule, closely associated with lipscombite, orange frondelite, and Fe-Mn oxide minerals (Fig. 4c). Tavorite also appears in beusite close to the contact with heterosite or ferrisicklerite, in association with pleochroic hureaulite (Fig. 4b); it may be replaced by phosphosiderite or robertsite-mitridatite.

Tavorite from association II does not show significant chemical variations; its composition is very close to the ideal formula, $LiFe^{3+}(PO_4)(OH)$ (Table 4). The chemical compositions of tavorite from association III show MnO contents from 0.48 to 7.70 wt.% MnO; however, such high contents may be due to contamination by surrounding minerals. Indeed, BSE images of tavorite reveal intergrowths with very small grains (less than 5 μm in width) of an undetermined species; this texture can be explained by a late replacement processes. The average composition of tavorite from association III, given in Table 4, must consequently be considered with caution.

Minerals of the rockbridgeite-frondelite series

Minerals of the rockbridgeite-frondelite series appear as large bottle-green fibroradial crystal aggregates (up to 3 cm in length), which imbricate with each

other, or as small fibroradial orange spheres (up to 2 mm in diameter). In association I, rockbridgeite-frondelite forms intergranular fibroradial masses between cleavelandite lamellae, in close association with minerals of the jahnsite group; rockbridgeite-frondelite may also replace barbosalite. The color of rockbridgeite-frondelite shows huge variations that are not directly correlated with the chemical composition. In some thin sections, rockbridgeite-frondelite grains are strongly pleochroic, passing from orange to deep bottle-green; some grains are less pleochroic or non-pleochroic, being almost opaque with dark brown or orange colors. In sample Joc-2, rockbridgeite-frondelite fans include tiny grains of greifensteinite, reddish sphalerite, or pyrite. In association II, rockbridgeite-frondelite forms fans of brownish orange to bottle-green fibroradial crystal aggregates, replacing barbosalite associated with hureaulite (Fig. 3b, c). Rockbridgeite-frondelite also appears as small dark fibroradial spheres (100 μm in diameter) with pleochroic rims (orange to bottle green); these spheres are stacked upon each other in the cleavage cracks of triphylite, form botryoidal masses in cavities, or occur on vivianite crystals. In association III, rockbridgeite-frondelite crystallizes as fibroradial aggregates of slightly pleochroic crystals (light orange to orange), on the border of the oxidized nodule margin; these aggregates are rimmed by garnet. In the same margin, orange non-pleochroic rockbridgeite-frondelite also forms a complex intimate intergrowth with tavorite, minerals from the mitridatite-robertsite series, scarce phosphosiderite, and Fe-Mn oxide minerals (Fig 4c).

Minerals of the rockbridgeite-frondelite series show a variation of their Fe/Mn ratio: the MnO content varies from *ca*. 4–11 wt.% MnO_{tot} while the FeO content fluctuates from *ca*. 40–50 wt.% FeO_{tot} in the three associations (Table 5). We calculated the cation number on the basis of 3P *pfu* and Fe^{3+} to maintain charge balance. In some cases, however, a small amount of Mn^{3+} was necessary to reach the total of 30 negative charges (Table 5). Baijot *et al*. (2012) explain this excess of negative charges by the same auto-oxidation process described above for barbosalite; the resulting new formula for rockbridgeite-frondelite is $M^{2+}{}_{1-x}M^{3+}{}_{x}Fe^{3+}{}_{4}(PO_4)_3O_x(OH)_{5-x}$, where *M* corresponds to Fe (rockbridgeite) or Mn (frondelite). The presence of Mn^{3+} in rockbridgeite was confirmed by Redhammer *et al*. (2006), who observed a strong Jahn-Teller distortion of the Fe2 site induced by this cation.

As noted previously, variation of pleochroism colors cannot be correlated with chemical variations. For example, in samples Joc-1 and Joc-7, pleochroic minerals of the rockbridgeite-frondelite series, occurring in albite (or cleavelandite), constantly show orange to bottle green colors, even if their chemical compositions vary from frondelite to rockbridgeite. However, in both samples, rockbridgeite-frondelite grains show compositions close to the boundary between the two species (Table 5). Moreover, a similar chemical composition is observed for strongly pleochroic frondelite from association III, and for small darker (nearly opaque) spheres of association II (Table 5). These variations of pleochroism color are certainly due to changes in the oxidation states of Fe and Mn. Fransolet (1976) also observed that minerals of the rockbridgeite-frondelite series progressively lose their intense pleochroism during oxidation, thus confirming this hypothesis.

Minerals of the jahnsite group

In association I, jahnsite *s.l*. appears as interganular fibroradial yellowish fans (up to 500 μm), occurring between lamella of cleavelandite or in albite. These fans are closely associated with minerals of the rockbridgeite-frondelite series, which have a similar habit compared to jahnsite *s.l*.. In association II, jahnsite *s.l*. occurs in the cleavage planes of ferrisicklerite, associated with dark frondelite (Fig. 3b, c, d). In the area close to the contact between ferrisicklerite and triphylite, jahnsite *s.l*. is not so abundant as in the cleavage planes of ferrisicklerite, but occurs in orthogonal cracks within triphylite, associated with dark frondelite (Fig. 3b). Jahnsite *s.l*. may also replace hureaulite, and phosphosiderite occasionally forms on this association.

The electron-microprobe compositions of jahnsite *s.l*. from association I show the presence of two potentially new species in the jahnsite group: "jahnsite-(MnMnFe)", ideally $MnMnFe^{2+}{}_2Fe^{3+}{}_2(PO_4)_4(OH_2)\bullet 8H_2O$, and "whiteite-(MnMnMg)", ideally, $MnMnMg_2Al_2(PO_4)_4(OH_2)\bullet 8H_2O$ (Table 5). Both species are non-pleochroic; "jahnsite-(MnMnFe^{2+})" is deep yellow, while "whiteite-(MnMnMg)" exhibits a lighter yellow color. It is noteworthy that the cationic ratio $(R^{2+} + R^{3+})/(Si + P)$ for these minerals is too high (*ca*. 1.52–1.70), compared to the 1.50 value for the ideal formula. This feature is certainly due to an analytical error related to the fibrous habit of these minerals. Jahnsite *s.l*. from association II occurs as larger crystals, and shows a $(R^{2+} + R^{3+})/(Si + P)$ ratio of 1.52, close to the ideal value. Its chemical composition corresponds to jahnsite-(MnMnMn), even if some analyses show a significant enrichment in Fe (Table 5).

Associated silicates and other minerals

As described above, the main minerals of the Jocão pegmatite association are albite, quartz, microcline, spodumene, muscovite, schorl, and garnet. Generally, schorl and spodumene do not occur directly in contact with the phosphate mineral nodules, even if in sample Joc-4, a small grain of schorl (50 μm in length) occurs in the saccharoidal albite matrix, in close association with apatite and garnet of association I. Electron-microprobe compositions (Table 6) show that schorl associated

with apatite and garnet is relatively richer in Fe and Al and poorer in Mg and Si, compared to the samples associated with host silicate minerals. Muscovite, which is directly associated with phosphate minerals from association I, appears in the albitic matrix, where it sometimes forms symplectitic textures with quartz. Muscovite may also crystallize perpendicularly to the contact with triphylite, and may be replaced by greenish chlorite. Muscovite associated with the host silicate minerals shows a slight variation of its FeO content (*ca*. 0.55–1.68 wt.% FeO), as does muscovite from association I (1.02–5.22 wt.% FeO). These last samples show higher Fe contents compared to muscovites from association II and to those associated with the host silicate minerals (Table 6).

Garnet forms unusual petrographic textures with phosphate minerals of associations I and III. In association I (sample Joc-10), garnet may form intergrowths with triphylite (Fig. 2b), may be completely enclosed by triphylite (Fig. 2e), or may form a rim surrounding

TABLE 5. CHEMICAL COMPOSITION OF MINERALS FROM THE ROCKBRIDGEITE (ROCK)-FRONDELITE (FRON) SERIES AND FROM THE JANHSITE (JAHN) GROUP (WHITEITE= WHIT), JOCÃO PEGMATITE, MINAS GERAIS, BRAZIL

Mineral	Rock	Fron	Fron	Rock	Fron	Fron	Fron	Fron	"Jahn"	"Whit"	Jahn	Jahn
Samples	a	b	c	d	e	f	g	h	i	j	k	l
Association	I	I	I	II	II	II	III	III	I	I	II	II
Number of analyses	3	5	9	2	5	7	2	3	8	8	10	5
SiO_2 (wt.%)	0.00	0.02	0.01	0.01	0.00	0.01	0.00	0.01	0.00	0.00	0.00	0.00
P_2O_5	32.63	33.23	32.61	33.59	33.70	32.98	33.99	32.95	33.53	36.83	33.19	33.85
Al_2O_3	0.10	0.32	0.05	0.04	0.00	0.01	0.00	0.01	0.63	14.40	0.00	0.00
Fe_2O_3*	49.14	52.04	47.40	54.02	48.73	50.52	51.56	49.43	12.04	-	18.04	19.61
FeO*	6.11	-	5.77	1.65	-	2.99	-	2.74	18.41	8.99	1.63	5.79
MgO	0.21	0.10	0.03	0.12	0.10	0.04	0.01	0.02	4.19	6.34	0.91	2.26
Mn_2O_3*	-	2.44	-	-	6.58	-	5.25	-	-	-	-	-
MnO*	3.69	3.55	6.71	4.34	3.55	6.33	3.05	7.69	12.34	16.81	28.97	20.86
ZnO	0.13	0.20	0.22	0.09	0.20	0.10	0.19	0.27	0.03	0.09	0.21	0.05
CaO	0.16	0.23	0.16	0.02	0.16	0.13	0.18	0.23	1.95	2.35	0.87	1.42
Na_2O	0.01	0.04	0.00	0.00	0.03	0.00	0.00	0.00	0.78	0.05	0.43	0.59
K_2O	0.01	0.02	0.00	0.00	0.02	0.01	0.00	0.01	0.01	0.00	0.00	0.00
H_2O**	6.90	7.03	6.90	7.11	7.13	6.98	7.19	6.97	19.15	21.04	18.96	19.33
Total	99.08	99.22	99.86	100.99	100.20	100.10	101.42	100.35	103.06	106.90	103.21	103.76
Si *apfu*	0.000	0.002	0.000	0.001	0.000	0.001	0.000	0.001	0.000	0.000	0.000	0.000
P	3.000	2.998	3.000	2.999	3.000	2.999	3.000	2.999	4.000	4.000	4.000	4.000
Al	0.012	0.040	0.015	0.005	0.000	0.001	0.000	0.001	0.105	2.177	0.000	0.001
Fe^{3+}	4.015	4.172	4.264	4.288	3.856	4.083	4.046	3.999	1.278	-	1.932	2.057
Fe^{2+}	0.556	-	-	0.145	-	0.269	-	0.246	2.169	0.964	0.195	0.681
Mg	0.034	0.016	0.028	0.019	0.015	0.007	0.002	0.004	0.878	1.213	0.193	0.471
Mn^{3+}	-	0.198	0.227	-	0.524	-	0.417	-	-	-	-	-
Mn^{2+}	0.339	0.322	0.157	0.388	0.320	0.576	0.270	0.701	1.475	1.827	3.494	2.466
Zn	0.010	0.016	0.012	0.007	0.016	0.008	0.015	0.022	0.003	0.008	0.022	0.005
Ca	0.018	0.027	0.035	0.002	0.018	0.015	0.020	0.027	0.294	0.322	0.133	0.211
Na	0.002	0.009	0.015	0.000	0.006	0.000	0.000	0.000	0.214	0.012	0.118	0.160
K	0.001	0.003	0.003	0.000	0.003	0.001	0.001	0.001	0.001	0.000	0.004	0.001
OH	5.000	5.000	5.000	5.000	5.000	5.000	5.000	5.000	2.000	2.000	2.000	2.000
Σ M	4.987	4.803	4.756	4.854	4.758	4.960	4.771	5.001	6.417	6.523	6.091	6.053
$Fe_{tot}/(Fe_{tot}+Mn_{tot})$	0.931	0.889	0.917	0.920	0.820	0.883	0.855	0.858	0.700	0.345	0.378	0.526

- : not determined

Number of cations was calculated on the basis of 3 (P+Si) per formula unit (*pfu*) for minerals of rockbridgeite and frondelite series, on the basis of 4 (P+Si) *pfu* jahnsite group minerals; * Fe^{3+} and Mn^{3+} is calculated to maintain the charge balance, ** H_2O content was calculated according to the ideal formulae.

a = Rockbridgeite, assemblage I, sample Joc-1 (in albite); b = Mn^{3+}-bearing frondelite, assemblage I, Joc-1, Joc-2, Joc-10b; c = Frondelite without Mn^{3+}, assemblage I, Joc-2, Joc-10b; d = rockbridgeite, assemblage II, joc-7; e = Mn^{3+}-bearing frondelite, assemblage II, Joc-7, Joc-9; f = Frondelite without Mn^{3+}, assemblage II, Joc-7, Joc-9; g : Mn^{3+}-bearing frondelite, assemblage III, Joc-13a; h = Frondelite without Mn^{3+}, assemblage III, Joc-13a; i = "Jahnsite-(MnMnFe^{2+})", assemblage I, Joc-1, Joc-10b; j = "Whiteite-(MnMnMg)", assemblage I, Joc-1, k = jahnsite-(MnMnMn), assemblage II, Joc-7, Joc-11; l = Fe^{2+}-rich jahnsite-(MnMnMn), assemblage II, Joc-7

TABLE 6. CHEMICAL COMPOSITION OF HOST SILICATE MINERALS [SCHORL (SRL-H), MUSCOVITE (MS), AND SPESSARTINE (SPS)] AND SILICATE MINERALS DIRECTLY ASSOCIATED WITH THE PHOSPHATE ASSEMBLAGE [SRL-P, MS-P, SPS-P, CHAMOSITE (CHM-P)], JOCÃO PEGMATITE, MINAS GERAIS, BRAZIL

Mineral	Srl-h	Srl-p		Ms-h	Ms-h	Ms-p	Ms-p		Sps-h	Sps-p	Sps-p	Sps-p		Chm-p
Samples	a	b		c	d	e	f		g	h	i	j		k
Association	-	I		-	-	I	II		-	I	I	III		I & II
Number of analyses	(7)	(3)		(7)	(6)	(21)	(2)		(8)	(4)	(22)	(11)		(14)
SiO_2 (wt.%)	35.98	34.33	SiO_2 wt.%	45.44	44.94	44.65	44.45		35.75	35.99	35.14	36.25		21.99
P_2O_5	0.01	0.04	P_2O_5	0.04	0.04	0.01	0.04		0.57	0.17	0.47	0.42		0.18
B_2O_3*	10.70	10.57	Al_2O_3	35.54	37.59	35.86	36.97		20.75	21.03	20.86	20.76		21.72
Al_2O_3	35.61	36.97	FeO***	1.60	0.61	2.56	1.31		20.38	14.80	19.20	20.27		41.57
FeO	11.92	12.54	Fe_2O_3***	-	-	-	-		1.33	2.15	2.20	1.50		-
MgO	2.57	1.08	MgO	0.23	0.01	0.13	0.07		0.17	0.10	0.13	0.12		0.77
MnO	0.20	0.36	MnO	0.04	0.02	0.09	0.05		22.44	27.72	22.86	22.99		2.19
ZnO	0.06	0.07	ZnO	0.02	0.05	0.05	0.02		0.04	0.03	0.01	0.06		0.40
CaO	0.03	0.08	CaO	0.00	0.00	0.00	0.00		0.20	0.16	0.20	0.20		0.02
Na_2O	1.73	1.91	Na_2O	0.57	0.68	0.43	0.57		0.04	0.02	0.02	0.02		0.01
Li_2O**	0.10	0.19	K_2O	10.68	10.34	10.65	10.37		0.00	0.00	0.00	0.00		0.00
K_2O	0.03	0.04	H_2O****	4.33	4.43	4.40	4.44		-	-	-	-		10.35
H_2O*	3.63	3.56	F	0.26	0.11	0.05	-		-	-	-	-		
F	0.13	0.17	F≡O	-0.11	-0.05	-0.02	-		-	-	-	-		
O≡F	-0.05	-0.07												
			Total	98.64	98.77	98.86	98.29		101.67	102.17	101.09	102.59		99.21
Total	102.65	101.84												
			$Si^{[4]}$ *apfu*	3.061	3.007	3.023	3.004	*T* : Si *apfu*	2.909	2.915	2.878	2.927	$Si^{[4]}$ *apfu*	2.547
T : Si *apfu*	5.842	5.648	$P^{[4]}$	0.002	0.002	0.001	0.002	P	0.039	0.012	0.032	0.029	$P^{[4]}$	0.017
P	0.001	0.006	$Al^{[4]}$	0.937	0.991	0.976	0.994	Al	0.052	0.073	0.090	0.044	$Al^{[4]}$	1.436
Al	0.157	0.346	$Al^{[6]}$	1.884	1.973	1.901	1.950	*Y* : Al	1.938	1.934	1.924	1.932	$Al^{[6]}$	1.527
B	3.000	3.000	Fe^{2+}	0.090	0.034	0.145	0.074	Fe^{3+}	0.081	0.066	0.076	0.090	Fe^{2+}	4.032
Z : Al	6.000	6.000	Mg	0.023	0.001	0.013	0.007	Σ *Y*	2.019	2.000	2.000	2.022	Mg	0.133
Y : Al	0.659	0.821	Mn	0.002	0.001	0.005	0.003	*X* : Fe^{2+}	1.387	1.002	1.315	1.369	Mn	0.215
Mg	0.622	0.266	Zn	0.001	0.002	0.002	0.001	Fe^{3+}	0.000	0.065	0.060	0.000	Zn	0.034
Fe^{2+}	1.619	1.725	Σ $X^{[6]}$	2.000	2.011	2.066	2.035	Mg	0.021	0.012	0.016	0.014	Ca	0.003
Mn	0.028	0.051	Ca	0.001	0.000	0.000	0.000	Mn	1.547	1.902	1.586	1.572	Na	0.003
Zn	0.007	0.009	Na	0.074	0.088	0.057	0.075	Zn	0.003	0.002	0.001	0.004	K	0.000
Li	0.065	0.128	K	0.918	0.883	0.920	0.894	Ca	0.017	0.014	0.018	0.017	Σ $X^{[6]}$	5.947
Σ *Y*	3.000	3.000	Σ	0.992	0.971	0.977	0.969	Na	0.006	0.004	0.004	0.003		
X : Ca	0.006	0.015						K	0.000	0.000	0.000	0.000		
Na	0.544	0.609						Σ *X*	2.981	3.001	3.000	2.979		
K	0.006	0.008	H	1.944	1.977	1.988	2.000							8.000
□	0.450	0.383	F	0.056	0.023	0.012	-							-
OH	3.935	3.912												
F	0.065	0.088												
$Fe_{tot}/(Fe_{tot}+Mn_{tot})$	0.982	0.971							0.487	0.373	0.478	0.481		
$Fe_{tot}/(Fe_{tot}+Mg)$	0.722	0.866							0.986	0.990	0.989	0.990		

- : not determined.

Cation numbers of schorl were calculated on the basis of 49 positive charges per formula unit, and all Fe and Mn were assumed to be divalent; *B_2O_3 and H_2O were calculated according to the ideal formula with (OH+F) = 4 *apfu*. ** Li was taken to be equal to the ideal sum of the Y crystallographic site minus the amount of other cations occupying those sites (Li = 3 – Y), and the calculation was iterated to self-consistency (Burns *et al.* 1994).

For the other silicates, cation numbers were calculated on the basis of 12 (O, OH) (muscovite), 8 cations (spessartine), 18 (O,OH) (chamosite) per formula unit, and ***Fe_2O_3 and FeO were calculated to maintain the charge balance, **** H_2O was calculated according to the ideal formula, with (OH+F) = 2 *apfu* for muscovite. a = Schorl, host silicates; b = Schorl associated with phosphate minerals of assemblage I; c = Muscovite relatively richer in iron, host silicates; d = Fe^{2+} free-muscovite, host silicates; e = Muscovite associated with phosphate minerals of assemblage I; f = Muscovite associated with phosphate minerals of assemblage II; g = Spessartine garnet, host silicates; h = Spessartine garnet associated with apatite without triphylite, Joc-4; i = Spessartine garnet, assemblage I, Joc 10, Joc12; j = Spessartine garnet, assemblage III, Joc-13; k = chamosite, assemblage I (Joc-2, Joc-10, Joc-12) and assemblage II (Joc-11)

triphylite (Fig. 2f). Moreover, in sample Joc-12, triphylite forms a rim surrounding garnet (Fig. 2c); in this last case, a rim of limpid quartz sometimes appears between the garnet and the triphylite, or between triphylite and the matrix. Garnet often shows quartz inclusions or exsolutions, forming a symplectitic texture (Fig. 2e). Chlorite sometimes occurs in cracks between garnet grains (Figs. 2b, 2e). Garnet is always associated with fluorapatite, but these two minerals are not present in association II. In association III, garnet crystallizes as a rim around the oxidized border of the phosphate mineral nodule (500 μm in width), in contact with an orange acicular frondelite layer. In this case, garnet seems to be replaced in the most external part of the rim by an undetermined anisotropic mineral. This rim is in contact with quartz. Garnet also occurs between two lamellae of heterosite, in association with apatite and harrisonite (Fig. 4d).

The chemical compositions of these garnets correspond to spessartine, with a high almandine component (Table 6). Spessartines associated with host silicate minerals, from association I and from association III, have similar chemical compositions, except in sample Joc-4 where this mineral is poorer in Fe and richer in Mn. In this last sample, spessartine occurs in contact with apatite in a silicate matrix (albite + quartz + microcline ± schorl) (Table 6).

Greenish chlorite replaces muscovite or occurs as isolated grains in frondelite from association II. In association I, chlorite fills cracks in spessartine or crystallizes at the junction between garnet and triphylite grains (Figs. 2c, 3a). The chemical compositions of chlorites from association I and II are shown in Table 6, and correspond to chamosite.

Pyrite and sphalerite may fill cracks or be deposited on phosphate minerals, while gahnite was found as small inclusions in heterosite lamellae of association III.

Discussion

Crystallization sequence of primary phosphate associations

As described above, the primary phosphate minerals occur in different types of associations: association I where triphylite is dendritic and shows intergrowths with silicate minerals (albite Fig. 2a, garnet, Fig. 2b), association II where triphylite occurs as massive nodules, and association III where triphylite forms exsolution lamellae in massive beusite. According to Keller (1988), these dendritic phosphates are always associated with albite (± quartz ± muscovite) and can be found in several zones of the pegmatite: the external inner zone, internal inner zone, fracture fillings in the inner zone, near the quartz core, and in the replacement unit. Keller (1988) mentions that in the same phosphate-bearing pegmatite the phosphate minerals display two kinds of habits, dendritic and blocky, the latter appearing in the inner internal zone along the core margin.

In the Jocão pegmatite, the phosphate nodules were collected from the dumps, so it is impossible to accurately identify the pegmatite zone from which they crystallized. However, it is possible to classify the phosphate mineral nodules on the basis of their differentiation, according to the hypothesis of Keller (1988). Indeed, if we consider that albite and triphylite crystallized simultaneously during the magmatic stage, these two minerals must appear in an outer zone, compared to the blocky phosphate minerals. This conclusion is confirmed by the fact that dendritic textures generally form under a high degree of undercooling, which is generally reached near the contact with the country rock (Keller 1988, London

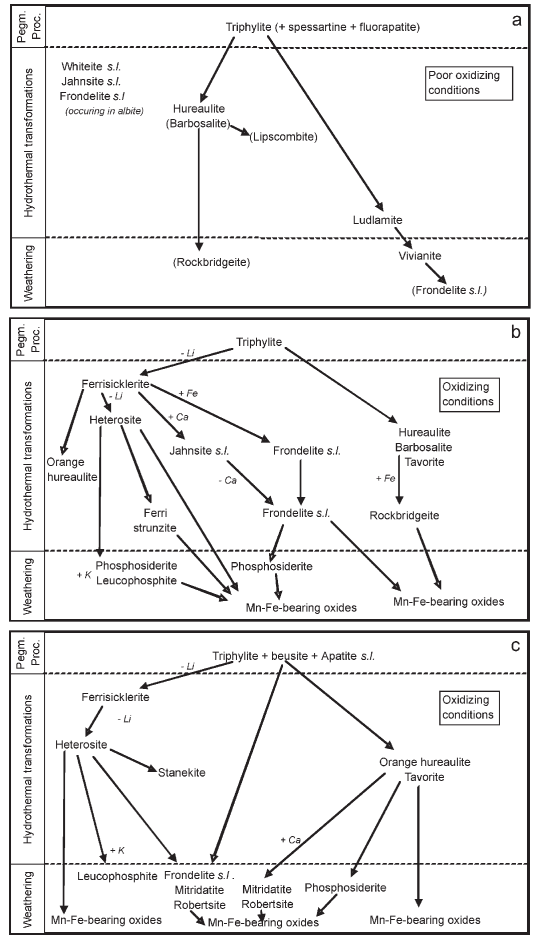

FIG. 5. Transformation sequence of phosphate minerals of association I (a), association II (b), and association III (c), Jocão pegmatite, Minas Gerais, Brazil.

1992, Simmons & Webber 2008). Moreover, the $Fe_{tot}/(Fe_{tot}+Mn_{tot})$ ratio of phosphate minerals must decrease in the pegmatite, from the margin to the core, according to general pegmatite differentiation geochemical trends (Ginsburg 1960, Simmons & Webber 2008). In the Cema pegmatite, Argentina, Roda-Robles *et al.* (2012) showed, however, that the $Fe_{tot}/(Fe_{tot}+Mn_{tot})$ ratio of phosphate minerals may also be strongly influenced by the abundance of associated Fe- and Mn-bearing silicate minerals.

The $Fe_{tot}/(Fe_{tot}+Mn_{tot})$ ratio of dendritic triphylite I is slightly higher (0.561) than that of blocky triphylite II (0.557 or 0.513), thus confirming that massive triphylite formed after the crystallization of the dendritic triphylite, from a more evolved magma. Triphylite occurring with garnet was not taken into account in this hypothesis, because garnet may influence the $Fe_{tot}/(Fe_{tot}+Mn_{tot})$ ratio of the triphylite. The electron-microprobe compositions of triphylite II indicate the presence of two generations of this mineral, characterized by $Fe_{tot}/(Fe_{tot}+Mn_{tot})$ ratios of 0.557 and 0.513, respectively (Table 3).

As discussed below, phosphate minerals in association III show exsolution textures, thus indicating the existence of a high-temperature precursor. The experimental data obtained by Hatert *et al.* (2014), from similar exsolution textures involving triphylite and sarcopside, confirm that these associations crystallized at high temperatures, between *ca.* 350 and 450 °C. Phosphate mineral nodules of association III should be considered as having crystallized in a zone where the undercooling was weaker. The $Fe_{tot}/(Fe_{tot}+Mn_{tot})$ ratios of ferrisicklerite and heterosite lamellae cannot be used to compare the evolutionary degree of the associations, since the presence of garnet may significantly influence this ratio.

Petrogenetic significance of the triphylite-garnet intergrowths

According to London *et al.* (1999), the crystallization of mafic silicate and phosphate minerals is sequential (*i.e.*, the phosphate minerals succeed the silicate minerals with little or no overlap in their paragenesis). Moreover, London *et al.* (1999) explained that an increase of P_2O_5 content in the melt may destabilize garnet, and then phosphate may crystallize following the reaction:

$$Mn_3Al_2(SiO_4)_3 + P_2O_5\ [\text{in the melt (m)}] \rightarrow Mn_3(PO_4)_2 + Al_2SiO_5\ (m) + SiO_2\ (m) \quad (1)$$

Vignola *et al.* (2008), who observed garnet forming a rim on graftonite + triphylite masses, or garnet included in graftonite, justify these textures by equation (1). In our case, however, due to the increase of Li_2O activity in the melt, triphylite would crystallize instead of graftonite, and would almost completely replace garnet, leaving only garnet relics in triphylite masses (Fig. 2e) or rims of garnet at the border of triphylite (Fig. 2f). Additionally, this replacement may be very limited, as a rim of triphylite may also appear in contact with garnet (Fig. 2c). Such a texture can be explained by the fact that during the crystallization of triphylite, P (but also Li) is progressively removed from the melt; when its activity becomes too low, there is no more P in the system to destabilize garnet and form triphylite.

It is noteworthy that Baijot *et al.* (2012) also observed a rim of garnet formed by a reaction between triphylite and albite during the albitization processes affecting the Sapucaia pegmatite. In the Jocão pegmatite described herein, we observed a rim of garnet around triphylite, but also garnet enclosed in triphylite without any contact with albite; the first explanation consequently seems more reasonable. Moreover, the enclosed garnet and the garnet constituting the rim have the same chemical composition, which would not probably be the case if the rim formed during the albitization processes. It is also important to note that reaction (1) provokes an excess of quartz in the melt, which explains the quartz inclusions in garnet (Fig. 2e), the abundance of quartz in the vicinity of garnet (Fig. 2b, f), and the rim of quartz frequently associated with the triphylite rim at the garnet border. These petrographic observations again confirm a reaction similar to that of equation (1).

Nevertheless, the hypothesis described above cannot explain the dendritic intergrowths of garnet and triphylite observed in some sample from Jocão (Fig. 2b). As mentioned by Keller (1988), intergrowths between dendritic triphylite and garnet only suggest a syn-crystallization or an overlapping during the crystallization time, with dendritic phosphate minerals growing from the melt, just before the beginning of silicate mineral crystallization.

In association I, fluorapatite, occurring as intergrowths with garnet and triphylite, probably crystallized at the same time as triphylite and garnet, while fluorapatite occurring in cracks with garnet (Fig. 2d), probably formed because of P-induced destabilization of garnet.

Transformation sequence of phosphate mineral associations

For each type of phosphate mineral association, the textural relationships observed in thin sections and described above allow one to establish the genetic sequence of Fe-Mn-bearing phosphate minerals, which is given in Figure 5.

In association I and II, triphylite is the main primary (magmatic) phosphate mineral, which crystallized during the Li-stage described by Ginsburg (1960). After this Li magmatic stage, triphylite was altered by hydrothermal processes and then replaced by several minerals under different physico-chemical conditions leading to mineral associations I and II.

Association I. In this association, triphylite first remained unaltered and was not affected by metasomatic and oxidation processes, which would lead to the formation of ferrisicklerite/heterosite and/or alluaudite. The first hydrothermal alteration stage was a weakly oxidizing hydroxylation event, during which triphylite was only replaced by hureaulite along the cleavage planes, or by an association of hureaulite and barbosalite (sample Joc-10). Normally, during this replacement process, the Fe/Mn ratio of primary triphylite is preserved: even if hureaulite and barbosalite are Mn- and Fe-rich phases, respectively, the average Fe/Mn ratio of the system remains relatively close to that of the parent triphylite (Quensel 1957, Moore & Molin-Case 1974, Fransolet *et al*. 1986, Baijot *et al*. 2012). In samples from Jocão, the chemical compositions and relative volumes of both secondary phases, barbosalite and hureaulite, vary significantly in the thin sections; it is consequently extremely difficult to accurately determine the average Fe/Mn ratio of the system, and to compare it with that of the triphylite. However, even if the hureaulite occurring without barbosalite (*i.e*., Fig. 2d) is relatively rich in Fe (Table 4, columns d, e), the Fe/Mn ratio of the hureaulite is significantly lower than that of the parent triphylite, thus showing that some Fe had to be removed from the system during the hydroxylation stage.

During a second low-temperature hydroxylation and oxidation stage, barbosalite is replaced by rockbridgeite, indicating enrichment in Fe. Jahnsite *s.l.* and frondelite *s.l.*, which occur between albite or cleavelandite grains, probably formed during an albitization stage. This event, which probably took place during the high-temperature hydroxylation stage, is difficult to locate accurately, since no direct contact between triphylite and interstitial phosphate mineral grains associated with albite were observed. The albitization stage is characterized by an increase in porosity, often coupled with the precipitation of other minerals between albite grains or in pores (Boulvais *et al*. 2007, Engvik *et al*. 2008, Putnis & Austrheim 2010); these features are similar to those observed in our sample. All elements (mainly P, Fe, Mn) were present in the solution to form hydrothermal minerals such as jahnsite *s.l.* and frondelite *s.l.*; this solution was weakly oxidizing since both Fe^{2+} and Fe^{3+} are present in these minerals. Aluminum, which is generally not considered to be very mobile, probably originated from the destabilization of previous microcline (or another aluminosilicate mineral) to form albite, and is consequently available to form whiteite *s.l.*.

Finally, during the meteoric processes, ludlamite and then vivianite, two ferrous highly-hydrated iron-bearing phosphate minerals, progressively replaced triphylite.

Association II. In this association, triphylite evolved under more oxidizing conditions. The first hydrothermal stage is the progressive oxidation of Fe and Mn in triphylite, coupled with a partial to complete Li-leaching, which caused the replacement of triphylite by ferrisicklerite and heterosite, successively, following the so-called Quensel-Mason sequence (Fig. 6, Quensel 1937, Mason 1941).

It is surprising to see, in the same pegmatite, both phosphate mineral nodules which remain composed of unaltered triphylite and phosphate mineral nodules completely replaced by ferrisicklerite or heterosite. This feature may indicate a significant variation of the local oxidation conditions, occurring during the high-temperature hydrothermal transformations. However, in the Sapucaia pegmatite, Baijot *et al*. (2012) observed a correlation between the size of the nodule and its mineralogical content: indeed, triphylite nodules are massive and can be more than 1 m in diameter, whereas ferrisicklerite nodules containing dendritic albite attain only a few cm in size. Consequently, small nodules are more affected by oxidation than large nodules, indicating that the diffusion kinetics are relatively low in these aggregates, thus oxidation is more difficult in the large nodules. This hypothesis is confirmed by the existence of intermediate nodules, which clearly show a progressive transition from unaltered triphylite (Fig. 3a) to ferrisicklerite (Fig. 3c) and then to heterosite (Fig. 3d).

The consequence of this hypothesis is that the phosphate mineral nodules clearly appear as a relatively closed system, compared to the silicate matrix. This closed system does not significantly interact chemically with the silicate minerals, since chemical reactions between phosphate and silicate minerals are relatively rare (except in the case of dendritic phosphate minerals, where the reactions are common due to the fine intergrowth of phosphate minerals with albite, Hatert *et al*. 2010, Baijot *et al*. 2012). Moreover, the high-temperature oxidizing hydrothermal solutions do not affect the phosphate mineral nodules homogeneously, due to their low diffusion kinetics, thus producing a triphylite (core)-ferrisicklerite-heterosite (rim) zoning (see below, Fig. 6). Finally, we observed, in association III (see below), a zoning of the proportions of beusite-heterosite lamellae in the exsolution textures, with *ca*. 24% heterosite in the core of the nodule, and *ca*. 29% at the border. Since Hatert *et al*. (2014) demonstrated experimentally that the proportions of phosphate minerals in the exsolution textures are correlated with the exsolution temperature, it appears that a temperature zoning also certainly exists within the phosphate nodules, with a lower temperature at the border, thus indicating that these nodules also constitute a relatively closed thermal system.

The second hydrothermal stage corresponds to a hydroxylation stage, like in association I. But here, the hydroxylated species are different, and depend on the previous phosphate mineral that they replace (Figs. 3, 6). In samples Joc-11 and Joc-7, we observe, in the same thin section, triphylite altered only to Fe^{2+}-Mn^{2+}-bearing hydrated species (colorless hureaulite); ferrisicklerite altered to Fe^{2+}-, Mn^{2+}-, and Fe^{3+}-bearing phosphate minerals such as jahnsite *s.l.*, frondelite

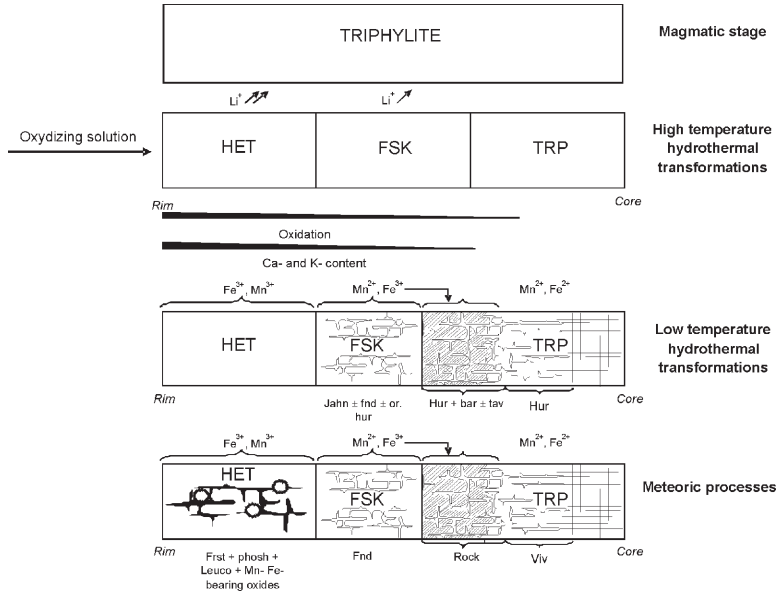

FIG. 6. Schematic transformation sequence of phosphate minerals from association II, with the different phosphate species formed during each stage affecting the nodule.

s.l., and orange hureaulite; and heterosite replaced by Fe^{3+}-bearing species like ferristrunzite. Consequently, it appears that the secondary phosphate minerals, which crystallize during this second hydrothermal stage, strongly depend on the cations which are locally available in the sample zone: in triphylite, Fe^{2+} is abundant, thus leading to the formation of Fe^{2+}-bearing hureaulite, whereas at the contact between triphylite and ferrisicklerite, both Fe^{2+} and Fe^{3+} are present, thus also producing barbosalite (Figs. 3a, 6). In ferrisicklerite, Mn^{2+} is present, producing jahnsite-group minerals, while in heterosite, Mn^{3+} is dominant, thus preventing the crystallization of secondary phosphate minerals at that stage (Mn^{3+}-bearing phosphate minerals are rare). It is noteworthy that the crystallization of jahnsite *s.l.* in ferrisicklerite is also certainly induced by the presence of significant amounts of Ca in this phosphate mineral, while it is virtually absent in triphylite.

Ferristrunzite is significantly more oxidized than hureaulite or jahnsite-group minerals, and contains large amounts of water molecules; for that reason, it is considered to form at a lower temperature. Ferristrunzite occurs along the cleavage planes of heterosite, thus indicating that it did not crystallize under meteoric conditions; we consequently decided to consider this species as forming between the low-temperature hydrothermal and the meteoric conditions (Fig. 5).

The final stage forms the meteoric species. During these replacements, the former textures are not preserved: leucophosphite and phosphosiderite directly replace heterosite, they do not occur in its cleavage planes, but are progressively "eating" the crystal (Fig. 6). Phosphosiderite may also be perched on frondelite fans. The Mn-Fe-bearing oxide minerals are the last species to form from heterosite, whereas vivianite, a ferrous meteoric species, only appears in the triphylite core. This feature confirms that the secondary species depend on the mineral which is altered. In sample Joc-9, small spheres of frondelite *s.l.* are perched on vivianite crystals, thus indicating that the oxidizing conditions significantly increased during the last meteoric stage.

Association III. This association is composed of massive beusite, forming lamellar intergrowths with ferrisicklerite and heterosite. These olivine-type phosphate minerals frequently occur as exsolution lamellae in masses of graftonite-beusite or in sarcopside masses (Hurlbut & Aristarain 1968, Moore 1972, Fransolet 1977, Wise & Černý 1990, Wise *et al.* 1990, Černý *et al.* 1998, Smeds *et al.* 1998, Galliski *et al.* 2009, Hatert *et al.* 2009, 2014, Roda *et al.* 2004, Roda-Robles *et al.* 2011, Vignola *et al.* 2011). Nevertheless, exsolution of a Fe-rich endmember-like heterosite into Mn-rich beusite is not common; it has only been observed in the Yellowknife pegmatite field, Canada, and in the Sidensjö and Stora Persholmen dikes in Sweden (Wise & Černý 1990, Smeds *et al.* 1998). These intergrowths of lithiophilite in beusite or triphylite in graftonite are most often interpreted as exsolution products by these authors, even if some of them suggest a Fe^{2+} or/and Li metasomatism (Fransolet 1977) or simultaneous crys-

tallization responsible for the graphic texture (Peacor 1969, Huvelin *et al.* 1971, Fransolet 1977).

At Jocão, the textural relationships between the lamellae of ferrisicklerite and heterosite in beusite correspond to an exsolution process, according to the criteria proposed by Schwartz (1942). These exsolution lamellae formed at the expense of a high-temperature homogenous Ca-Li bearing graftonite-beusite-like phase; when the temperature fell, Li migrated into triphylite and Ca to the larger M1 site of beusite. The bulk composition of the high-temperature homogenous phase, calculated from the relative volume proportions, the densities, and the chemical compositions of triphylite and beusite, corresponds to $(Mn_{1.25}Fe^{2+}_{1.07}Li_{0.54}Ca_{0.40}Mg_{0.04}Fe^{3+}_{0.02}Zn_{0.01})_{\Sigma 3.33}(P_{0.99}O_4)_2$, and contains significant amounts of Fe^{2+} and Mn. Moreover, the values of $K_{Fe\ beu/trp}$ (average 0.772) and $K_{Mn\ beu/trp}$ (average 1.343) clearly show that Fe has partitioned preferentially to the M2 octahedral site of the triphylite structure, and Mn to the larger seven-coordinated M1 site of the beusite structure, as was previously observed by several authors (Wise & Černý 1990, Smeds *et al.* 1998, Roda-Robles *et al.* 2011, Tait *et al.* 2013). Consequently, as the temperature fell, the precursor formed exsolution lamellae of triphylite into beusite; however, a precursor richer in Mn would have formed exsolution lamellae of lithiophilite in beusite (Hurlbut & Aristarain 1968, Smeds *et al.* 1998, Galliski *et al.* 2009), and a precursor richer in Fe would have produced exsolution lamellae of triphylite into graftonite (Smeds *et al.* 1998).

In the pegmatitic context, several authors agree that graftonite-beusite crystallized in LCT pegmatites during the magmatic stage, before the Li stage and the crystallization of triphylite (Huvelin *et al.* 1971, Fransolet 1977, Smeds *et al.* 1998). Moreover, Smeds *et al.* (1998) explained that similar Fe/Mn ratios in garnet and phosphate mineral associations indicate that these phosphate minerals crystallize because of P enrichment in the melt, inducing a destabilization of garnet (London *et al.* 1995, 1999). In Jocão, the Fe/(Fe+Mn+Mg) ratio of garnet occurring in association III is 0.479; if we consider the average values of 27 vol.% triphylite and 73 vol.% of beusite in the phosphate mineral association, the Fe/(Fe+Mn+Mg) ratio of the precursor phase is 0.457, which is very close to that of associated garnet, thus indicating that the differentiation degree of the melt was similar during the crystallization of garnet and phosphate minerals. We can consequently consider that the phosphate mineral precursor crystallized immediately after the destabilization of garnet, when the P_2O_5 activity increased in the melt.

The high-temperature hydrothermal alteration process begins after the magmatic phase. During this stage, triphylite transforms into ferrisicklerite and heterosite, following the Quensel-Mason sequence, as in association II (see above); however, beusite is not affected by any transformation process at this stage. It is noteworthy that the transformation processes affected the border of the nodule more intensely, where heterosite occurs, than the core of the nodule, where ferrisicklerite is the only observed phase.

During the low-temperature hydroxylation stage, ferrisicklerite from the core remains almost unaltered, while beusite is replaced by an intimate mixture of pleochroic Ca-rich hureaulite and tavorite. As mentioned by Mason (1941) and Vignola *et al.* (2011), who described respectively the alteration processes of graftonite and of a triphylite + sarcopside + graftonite association, Ca is leached out of beusite during the hydroxylation stage. The availability of Ca explains the crystallization of Ca-rich hureaulite during that stage (Table 4); however, we have to be careful with these chemical analyses, since hureaulite and tavorite are fine grained and later replaced by Ca-bearing mitridatite-robertsite. Due to this possible contamination, it is also difficult to affirm that the Fe/Fe+Mn ratio is preserved during this early phase of alteration, as observed in the Luna pegmatite (Vignola *et al.* 2011).

After this hydroxylation stage, the meteoric stage is characterized by an increase in Ca^{2+} and H_2O activities, responsible for the replacement of hureaulite and tavorite by mitridatite-robertsite. It is noteworthy that a second generation of robertsite forms veinlets crosscutting all previous minerals, including hureaulite, tavorite, as well as the first generation of mitridatite-robertsite. At the border, beusite and heterosite are completely replaced by an intimate mixture mainly constituted by frondelite and robertsite-mitridatite. At the contact between the oxidized border and the core of the nodule, petrographic textures are preserved, even if heterosite lamellae are replaced by (Mn-Fe)-bearing oxides (Fig. 4c); however, the lamellar texture disappears at the rim of the nodule, due to the formation of very late secondary minerals.

In association III, we observed a rare silico-phosphate mineral, harrisonite, $Ca(Fe^{2+},Mg)_6(SiO_4)_2(PO_4)_2$, which was previously reported from an Fe-silicate-quartz-apatite layered body found in granulite-facies gneisses on Arcedeckne Island (Grice & Roberts 1993, Roberts *et al.* 1993), in a quartz-garnet-rich rock (garnetite) associated with a paragneiss metamorphosed in the upper amphibolite facies (Verpaelst *et al.* 2001), and in a pegmatite from the Czech Republic (Škoda *et al.* 2007). Škoda *et al.* (2007) observed this mineral in phosphate mineral nodules as minute inclusions in graftonite, associated with sarcopside, wolfeite, triphylite, monazite-(Ce), and xenotime-(Y); however, they did not determine the genetic position of harrisonite in the phosphate mineral transformation sequence. In the Jocão pegmatite, harrisonite is associated with garnet, without any replacement texture, thus indicating that the mineral is primary and certainly crystallized shortly after the formation of garnet and before the formation of beusite. The Fe/(Fe+Mn+Mg) ratio of harrisonite

(0.801) is significantly higher than that of garnet (0.475), showing that Fe is preferentially partitioned into harrisonite, compared to garnet.

Crystal-chemical considerations for triphylite-type phosphate minerals

Olivine-type phosphate minerals of the Quensel-Mason sequence, described in this paper, show unusual chemical features. First, the relatively high SiO_2 content of some phosphate grains, which can reach 0.95 wt.% SiO_2 in ferrisicklerite and 1.06 wt.% SiO_2 in heterosite (the highest content is 1.40 wt.% SiO_2). Most natural triphylites have an SiO_2 content below 0.5 wt.% SiO_2 (Fransolet *et al*. 1985, 1986, Li & Shinno 1997, Losey *et al*. 2004, Vignola *et al*. 2008, Galliski *et al*. 2009) even if most authors did not measure the SiO_2 content in their samples (Quensel 1937, Mason 1941, Fransolet 1980, Fransolet *et al*. 1984, Keller & Von Knorring 1989, Wise & Černý 1990, Keller *et al*. 1994, Černý *et al*. 1998, Smeds *et al*. 1998, Roda *et al*. 2004, Vignola *et al*. 2011). It is interesting to note that high SiO_2 contents were also observed in a lithiophilite from Los Aleros, Argentina (0.78 wt.% SiO_2; Hurlbut & Aristarain 1968), as well as in triphylite from the Pøibyslavice metagranite, Czech Republic (2–11 wt.% SiO_2; Škoda *et al*. 2013). Škoda *et al*. (2013) explained this high Si content by a solid solution between triphylite and fayalite, Fe_2SiO_4; however, the SiO_2 increase is also accompanied by an increase of the $Fe_3(PO_4)_2$ component (sarcopside), thus leading to the theoretical endmember $Fe_5(PO_4)_2(SiO_4)$. The substitution mechanism, which explains the solid solution between triphylite and $Fe_5(PO_4)_2(SiO_4)$, corresponds to $3Li^+ + P^{5+} = \square + 2Fe^{2+} + Si^{4+}$. This substitution mechanism is confirmed in the phosphate minerals from Jocão, since ferrisicklerite and heterosite of association III, which have the highest Fe content, also present the highest SiO_2 content (Table 3).

Another interesting feature of the olivine-type phosphate minerals from Jocão concerns the evolution of CaO and K_2O contents during the Quensel-Mason sequence, which increase significantly when triphylite is replaced by ferrisicklerite and heterosite. Indeed, the K contents of the samples investigated herein reach maximal values of 0.01 wt.% K_2O in triphylites, 0.04 wt.% K_2O in ferrisicklerites, and 0.14 wt.% K_2O in heterosite; a similar behavior is observed for Ca, which reaches maximal values of 0.04 wt.% CaO in triphylites, 0.14 wt.% CaO in ferrisicklerites, and 0.31 wt.% CaO in heterosites (Table 3). Schmid-Beurmann *et al*. (2013) produced ferrisicklerite hydrothermally, by low-temperature oxidation of triphylite, and observed the same increase of K_2O in synthetic ferrisicklerite. These authors explain that the K increase is governed by crystal-chemical constraints, and is necessary to stabilize the ferrisicklerite (and heterosite) structure. On the other hand, a similar increase of CaO was previously observed by different authors in natural phosphate minerals (Fontan *et al*. 1976, Fransolet *et al*. 1985, 1986).

Acknowledgements

This paper is dedicated to André-Mathieu Fransolet, Paul Keller, and François Fontan, for their outstanding contribution to the petrography, mineralogy, and crystal chemistry of pegmatite phosphate minerals. We would like to thank particularly André-Mathieu, who was director of the Laboratory of Mineralogy, University of Liège, for more than 20 years, and incited us to discover the complex but fascinating world of phosphate minerals. Maxime Baijot thanks the FNR (Luxembourg) for PhD grant EXT-BFR07-137 TR.

References

Baijot, M., Hatert, F., & Philippo, S. (2012) Mineralogy and geochemistry of phosphates and silicates in the Sapucaia pegmatite, Minas Gerais, Brazil: genetic implications. *Canadian Mineralogist* **50**, 1531–1554.

Boulvais, P., Ruffet, G., Cornichet, J., & Mermet, M. (2007) Cretaceous albitization and dequartzification of Hercynian peraluminous granite in the Salvezines Massif (French Pyrénées). *Lithos* **93**, 89–106.

Burns, P.C., MacDonald, D.J., & Hawthorne, F.C. (1994) The crystal chemistry of manganese-bearing elbaite. *Canadian Mineralogist* **32**, 31–41.

Čech, F., Padera, K., & Povondra, P. (1961) Lipscombite from pegmatites at Otov near Domazlice. *Acta Universitatis Carolinae Geologica* **3**, 171.

Čech, F., Johan, Z., & Povondra, P. (1972) La barbosalite de la pegmatite d'Angarf-Sud, plaine de Tazenakht, Anti-Atlas, Maroc. *Notes du Service Géologique du Maroc* **32**, 121.

Černý, P., Selway, J.B., Ercit, T.S., Breaks, F.W., Anderson, A.J., & Anderson, S.D. (1998) Graftonite-beusite in granitic pegmatites of the Superior Province: a study in contrasts. *Canadian Mineralogist* **36**, 367–376.

Chaves, M.L. & Scholz, R. (2008) Pegmatito Gentil (Mendes Pimentel, MG) e suas paragêneses mineralógicas de fosfatos raros. *Revista Escola de Minasde Ouro Preto* **61(2)**, 141–149.

Chaves, M.L., Scholz, R., Atencio, D., & Karfunkel, J. (2005) Assembléias e paragêneses minerais singulares nos pegmatitos de região de Galiléia (Minas Gerais). *Geociências* **24(2)**, 143–161.

Correia Nevez, J.M., Pedrosa Soares, A.C., & Marciano, V.R.P.R.O. (1986) A provincia pegmatítica oriental do Brazil à luz dos conhecimentos atuais. *Revista Brasileira de Geociências* **16**, 106–118.

ENGVIK, A.K., PUTNIS, A., FITZGERALD, J.D., & AUSTRHEIM, H. (2008) Albitization of granitic rocks: the mechanism of replacement of oligoclase by albite. *Canadian Mineralogist* **46**, 1401–1415.

FONTAN, F., HUVELIN, P., ORLIAC, M., & PERMINGEAT, F. (1976) La ferrisicklerite des pegmatites de Sidi-bou-Othmane (Jebilet, Maroc) et le groupe des minéraux à structure de triphylite. *Bulletin de la Société Française Minéralogie Cristallographie* **99**, 274–286.

FRANSOLET, A.-M. (1975) *Etude minéralogique et pétrologique des phosphates de pegmatites granitiques*. Ph.D. thesis, University of Liège, 333.

FRANSOLET, A.-M. (1976) L'huréaulite: ses propriétés minéralogiques et son rôle dans l'évolution génétique des phases Li(Fe,Mn)PO_4. *Bulletin de la Société Française Minéralogie Cristallographie* **99**, 261–273.

FRANSOLET, A.-M. (1977) Intercroissance et inclusions dans les associtations graftonite-sarcopside-triphylite. *Bulletin Société Française Mineralogie Cristallographie* **100**, 198–207.

FRANSOLET, A.-M. (1980) The eosphorite-childrenite series associated with the Li–Mn–Fe phosphate minerals from the Buranga pegmatite, Rwanda. *Mineralogical Magazine* **43**, 1015–1023.

FRANSOLET, A.-M. (2007) Phosphate associations in the granitic pegmatites: the relevant significance of these accessory minerals. *In* Granitic pegmatites: The state of the Art, International symposium, Porto, Portugal. Abstract volume, **7–8**.

FRANSOLET, A.-M., ANTENUCCI, D., SPEETJENS, J.-M., & TARTE, P. (1984) An X-ray determinative method for the divalent cation ratio in the triphylite-lithiophilite series. *Mineralogical Magazine* **48**, 373–381.

FRANSOLET, A.-M., ABRAHAM, K., & SPEETJENS, J.-M. (1985) Evolution génétique et signification des associations de phosphates de la pegmatite d'Angarf-Sud, plaine de Tazenakht, Anti-Atlas, Maroc. *Bulletin de Minéralogie* **108**, 551–574.

FRANSOLET, A.-M., KELLER, P., & FONTAN, F. (1986) The phosphate mineral associations of the Tsaobismund pegmatite, Namibia. *Contributions to Mineralogy and Petrology* **92**, 502–517.

GALLISKI, M.A., OYARZÁBAL, J.C., MÁRQUEZ-ZAVALÍA, M.F., & CHAPMAN, R. (2009) The association qingheiite-beusite-lithiophilite in the Santa Ana pegmatite, San Luis, Argentina. *Canadian Mineralogist* **47**, 1213–1223.

GINSBURG, A.I. (1960) Specific geochemical features of the pegmatitic process. *21st International Geological Congress Session Norden Report* **17**, 111–121.

GHEITH, M.A. (1953) Lipscombite: a new synthetic "iron lazulite". *American Mineralogist* **38**, 612.

GRICE, J.D. & ROBERTS, A.C (1993) Harrisonite, a well-ordered silico-phosphate with layered crystal structure. *Canadian Mineralogist* **31**, 781–785.

HATERT, F., OTTOLINI, L., KELLER, P., & FRANSOLET, A.-M. (2009) Crystal chemistry of lithium in pegmatite phosphates: A SIMS investigation of natural and synthetic samples. *Estudos Geológicos* **19**, 131–134.

HATERT, F., BAIJOT, M., PHILIPPO, S., & WOUTERS, J. (2010) Qingheiite-(Fe^{2+}), $Na_2Fe^{2+}MgAl(PO_4)_3$, a new phosphate mineral from Sebastião Cristino pegmatite, Minas Gerais, Brazil. *European Journal of Mineralogy* **22**, 459–467.

HATERT, F., OTTOLINI, L., FONTAN, F., KELLER, P., RODA-ROBLES, E., & FRANSOLET, A.-M. (2011) The crystal chemistry of olivine-type phosphates. *Geológica Argentina, Serie D, Publicación Especial* **14**, 103–105.

HATERT, F., RODA-ROBLES, E., OTTOLINI, L., SCHMID-BEURMANN, P., BAIJOT, M., & DAL BO, F. (2014) An experimental investigation of the triphylite + sarcopside assemblage: geothermometric applications to natural pegmatite phosphates. *Contributions to Mineralogy and Petrology* (in press).

HURLBUT, C.S. & ARISTARAIN, L.F. (1968) Beusite, a new mineral from Argentina, and the graftonite-beusite series. *American Mineralogist* **53**, 1799–1814.

HUVELIN, P., ORLIAC, M., & PERMINGEAT, F. (1971) Graftonite et sarcopside de Sidi-bou-Othmane (Jebilet, Maroc). *Notes du Service Géologique du Maroc* **31**, 277–284.

KELLER, P. (1988) Dendritic phosphate minerals and their paragenetic relation to the silicate minerals of pegmatites from Namibia and from the Black Hills, South Dakota, U.S.A. *Neues Jahrbuch für Minerlogie Abhandlungen* **159 (3)**, 249–281.

KELLER, P. & VON KNORRING, O. (1989) Pegmatites at the Okatjimukuju farm, Karibib, Namibia. Part I: Phosphate mineral associations of the Clementine II pegmatite. *European Journal of Mineralogy* **1**, 567–593.

KELLER, P., FRANSOLET, A.-M., & FONTAN, F. (1994) Triphylite-lithiophilite and triplite-zwieselite in granitic pegmatites: Their textures and genetic relationships. *Neues Jahrbuch für Mineralogie Abhandlungen* **168**, 127–145.

KELLER, P., FONTAN, F., ROLDAN, F.V., & DE PARSEVAL, P. (2007) Joosteite, Mn^{2+} (Mn^{3+}, Fe^{3+})(PO_4)O: a new phosphate mineral from the Helikon II Mine, Karibib, Namibia. *Neues Jahrbuch für Mineralogie Abhandlungen* **183**, 197–201.

LI, Z. & SHINNO, I. (1997) Next nearest neighbor effects in triphylite and related phosphate minerals. *Mineralogical Journal* **19**, 99–107.

LINDBERG, M.L. & PECORA, W.T. (1954) Tavorite and barbosalite: two new phosphate minerals from Minas Gerais, Brazil. *Science* **119**, 739.

LINDBERG, M.L. & PECORA, W.T. (1955) Tavorite and barbosalite: two new phosphate minerals from Minas Gerais, Brazil. *American Mineralogist* **119**, 952–966.

LONDON, D. (1992) The application of experimental petrology to the genesis and crystallization of granitic pegmatites. *Canadian Mineralogist* **30**, 499–540.

LONDON, D., WOLF, M.B., & MORGAN VI, G.B. (1995) Silicate + phosphate equilibria in peraluminous granites and pegmatites: monitors and buffers of P_2O_5 in melt. *Geological Society of America*, *Abstract Programs* **27**, 411.

LONDON, D., WOLF, M.B., MORGAN VI, G.B., & GALLEGO GARRIDO, M. (1999) Experimental silicate-phosphate equilibria in peraluminous granitic magmas, with a case study of the Albuquerque batholith at Tres Arroyos, Badajoz, Spain. *Journal of Petrology* **40**, 215–240.

LOSEY, A., RAKOVAN, J., HUGES, J.M., FRANCIS, C.A., & DYAR, M.D. (2004) Structural variation in the lithiophilite-triphylite series and other olivine-group structures. *Canadian Mineralogist* **42**, 1105–1115.

MASON, B. (1941) Minerals of the Varuträsk pegmatite. XXIII. Some iron-manganese phosphate minerals and their alteration products, with special reference to material from Varuträsk. *Geologiska Föreningen Förhandlinger* **63(2)**, 117–175.

MOORE, P.B. (1971) The $Fe^{2+}{}_3(H_2O)_n(PO_4)_2$ homologous series: crystal chemical relationships and oxidized equivalents. *American Mineralogist* **56**, 1–17.

MOORE, P.B. (1972) Sarcopside: Its atomic arrangement. *American Mineralogist* **57**, 24–35.

MOORE, P.B. (1982) Pegmatite minerals of P(V) and B(III). *In* Short course in granitic pegmatites in science and industry (P. Černý, ed.). *Mineralogical Association of Canada, Short Course Handbook* **8**, 267–291.

MOORE, P.B. & MOLIN-CASE, J. (1974) Contribution to pegmatite phosphate giant crystal paragenesis: II. The crystal chemistry of wyllieite, $Na_2Fe^{2+}{}_2Al(PO_4)_3$, a primary phase. *American Mineralogist* **59**, 280–290.

NALINI, H.A. (1997) *Caractérisation des suites magmatiques néoprotérozoïques de la région de Conselheiro Pena et Galiléia (Minas Gerais, Brésil): étude géochimique et structurale des suites de Galiléia et Urucum et leur relation avec les pegmatites à éléments rares associées.* Unpublished Ph.D. thesis, Ecole des mines de Saint Etienne et Ecole des mines de Paris, 237pp.

NALINI, H.A., BILAL, E., PAQUETTE, J.-L., PIN, C., & RÔMULO, M. (2000) Géochronologie U–Pb et géochimie isotopique Sr–Nd des granitoïdes néoprotérozoïques des suites Galiléia et Urucum, vallée du Rio Doce, Sud-Est du Brésil. *Comptes Rendus de l'Académie de Sciences, Sciences de la Terre et des Planètes* **331**, 459–466.

PAIVA, G. (1946) Província pegmatíticas do Brazil. *Boletim DNPM-DFMP* **78**, 13–21.

PEACOR, D.R. (1969) Triphylite–sarcopside–graftonite intergrowths from Custer, South Dakota. *American Mineralogist* **54**, 969–972.

PEDROSA-SOARES, A.C., NOCE, C.M., WIEDEMANN, C.M., & PINTO, C.P. (2001) The Araçuaí-West-Congo Orogen in Brazil: an overview of confined orogen formed during Gondwanaland assembly. *Precambrian Research* **110**, 307–323.

PEDROSA-SOARES, A.C., CHAVES, M., & SCHOLZ, R. (2009) Eastern Brazilian pegmatite province. *4th International Symposium on Granitic Pegmatites, Field trip guide*, 1–28.

PEDROSA-SOARES, A.-C., DE CAMPOS, C.P., NOCE, C., SILVA, L.C., NOVO, T., RONCATO, J., MEDEIROS, S., CASTEÑADA, C., QUEIROGA, G., DANTAS, E., DUSSIN, I., & ALKMIM, F. (2011) Late Neoproterozoic-Cambrian granitic magmatism in the Araçuaí orogen (Brazil), the Eastern Brazilian Pegmatite Province and related resources. *In* Granite-Related Ore Deposits (A.N. Sial, J.S. Bettencourt, C.P. De Campos, & V.P. Ferreira, eds.). *Geological Society, London, Special Publications* **350**, 25–51.

PUTNIS, A. & AUSTRHEIM, H. (2010) Fluid-induced processes: metsomatism and metamorphism. *Geofluids* **10**, 254–269.

PUTZER, H. (1976) *Metallogenetische Provinzen in Südamerika*. Schweizerbart'sche Verlagsbuchhandlung, Stuttgart, Germany, 316.

QUENSEL, P. (1937) Minerals of the Varuträsk pegmatite. I: The lithium-manganese phosphates. *Geologiska Föreningen Förhandlinger* **59**, 77–96.

QUENSEL, P. (1957) The paragenesis of the Varuträsk pegmatite, including a review of its mineral assemblage. *Arkiv Foer Kemi, Mineralogi och Geologi* **2(2)**, 9–125.

REDHAMMER, G.J., ROTH, G., TIPPELT, G., BERNROIDER, M., LOTTERMOSER, W., AMTHAUER, G., & HOCHLEITNER (2006) Manganoan rockbridgeite $Fe_{4.32}Mn_{0.62}Zn_{0.06}(PO_4)_3(OH)_5$: structure analysis and ^{57}Fe Mössbauer spectroscopy. *Acta Crystallographica* **C62**, i24–i28.

ROBERTS, A.C., STIRLING, J.A.R., GRICE, J.D., FRISCH, T., HERD, R.K., & JAMBOR, J.L. (1993) Harrisonite, a new calcium iron silicate-phosphate from Arcedeckne Island, District of Franklin, Artic Canada. *Canadian Mineralogist* **31**, 775–780.

RODA, E., PESQUERA, A., FONTAN, F., & KELLER, P. (2004) Phosphate mineral associations in Cañada pegmatite (Salamanca, Spain): Paragenetic relationschips, chemical compositions, and implications for pegmatite evolution. *American Mineralogist* **89**, 110–125.

RODA-ROBLES, E., GALLISKI, M., NIZAMOFF, J., SIMMONS, W., KELLER, P., FALSTER, A., & HATERT, F. (2011) Cation partitioning between minerals of the triphylite ± graftonite ± sarcopside association in granitic pegmatites. *Asociación Geológica de Argentina, Serie D, Publicación Especial* **14**, 161–164.

Roda-Robles, E., Galliski, M.A., Roquet, M.B., Hatert, F., & De Parseval, P. (2012) Phosphate nodules containing two distinct assemblages in the Cema granitic pegmatite, San Luis province, Argentina: paragenesis, composition and significance in the pegmatite evolution. *Canadian Mineralogist* **50**, 913–931.

Schmid-Beurmann, P., Ottolini, L., Hatert, F., Geisler, T., Huyskens, M., & Kahlenberg, M. (2013) Topotactic formation of ferrisicklerite from natural triphylite under hydrothermal conditions. *Mineralogy and Petrology* **107**, 501–515.

Schwartz, G.M. (1942) Progress in the study of exsolution in ore minerals. *Economic Geology* **37**, 345–378.

Simmons, W.B.S. & Webber, K.L. (2008) Pegmatite genesis: state of the art. *European Journal of Mineralogy* **20**, 421–438.

Škoda, R., Staněk, J., & Čopjaková, R. (2007) Minerální asociace fosfátových nodulí z granitického pegmatitu od cyrilova u velkého meziříčí, moldanubikum; Část I primární a exsoluční fáze. *Acta Musei Moraviae, Scientiae Geologicae* **92**, 59.–74.

Škoda, R., Novák, M., Havránek, V., & Lens, C. (2013) Solid solutions between silicate and phosphate minerals of the olivine structure type: Example from Pøibyslavice metagranite, Czech Republic. GAC-MAC 2013, Winnipeg 2013, Abstracts, 178–179.

Smeds, S.-A., Uher, P., Černý, P., Wise, M.A., Gustafsson, L., & Penner, P. (1998) Graftonite-beusite in Sweden: Primary phases, products of exsolution, and distribution in zoned populations of granitic pegmatites. *Canadian Mineralogist* **36**, 377–394.

Tait, K.T., Hawthorne, F.C., & Wise, M.A. (2013) The crystal chemistry of the graftonite-beusite minerals. *Canadian Mineralogist* **51**, 653–662.

Verpaelst, P., Brisebois, D., Perreault, S., Sharma, K.N.M., & David, J. (2001) Geology of the Koroc River area and part of the Hébron area (NTS 24I and 14L). *Ministère des Richesses Naturelles, Québec* **RG 2000-02**.

Vignola, P., Diella, V., Oppizzi, P., Tiepolo, M., & Weiss, S. (2008) Phosphate assemblages from the Brissago granitic pegmatite, Western Southern Alps, Switzerland. *Canadian Mineralogist* **46**, 635–650.

Vignola, P., Diella, V., Ferrari, E.S., & Fransolet, A.-M. (2011) Complex mechanisms of alteration in graftonite + sarcopside + triphylite association from Luna pegmatite, Piona, Lecco province, Italy. *Canadian Mineralogist* **49**, 765–776.

Wise, M.A. & Černý, P. (1990) Beusite-Triphylite intergrowths from the Yellowknife pegmatite field, Northwest Territories. *Canadian Mineralogist* **28**, 133–139.

Wise, M.A., Hawthorne, F.C., & Černý, P. (1990) Crystal structure of a Ca-rich beusite from Yellowknife pegmatite field, Northwest Territories. *Canadian Mineralogist* **28**, 141–146.

Received January 8, 2014. Revised manuscript accepted March 24, 2014.